

Standardizing Platinum Dainotti-correlated gamma-ray bursts, and using them with standardized Amati-correlated gamma-ray bursts to constrain cosmological model parameters

Shulei Cao ,^{1*} Maria Dainotti ,^{2,3†} Bharat Ratra ^{1‡}

¹*Department of Physics, Kansas State University, 116 Cardwell Hall, Manhattan, KS 66506, USA*

²*National Astronomical Observatory of Japan, 2-21-1 Osawa, Tokyo 181-8588, Japan*

³*Space Science Institute, Boulder, CO 80301, USA*

Accepted XXX. Received YYY; in original form ZZZ

ABSTRACT

We show that the Platinum gamma-ray burst (GRB) data compilation, probing the redshift range $0.553 \leq z \leq 5.0$, obeys a cosmological-model-independent three-parameter fundamental plane (Dainotti) correlation and so is standardizable. While they probe the largely unexplored $z \sim 2.3 - 5$ part of cosmological redshift space, the GRB cosmological parameter constraints are consistent with, but less precise than, those from a combination of baryon acoustic oscillation (BAO) and Hubble parameter [$H(z)$] data. In order to increase the precision of GRB-only cosmological constraints, we exclude common GRBs from the larger Amati-correlated A118 data set composed of 118 GRBs and jointly analyze the remaining 101 Amati-correlated GRBs with the 50 Platinum GRBs. This joint 151 GRB data set probes the largely unexplored $z \sim 2.3 - 8.2$ region; the resulting GRB-only cosmological constraints are more restrictive, and consistent with, but less precise than, those from $H(z) + \text{BAO}$ data.

Key words: cosmological parameters – dark energy – cosmology: observations – gamma-ray bursts

1 INTRODUCTION

Currently accelerated cosmological expansion and other cosmological observations are reasonably well accommodated in the spatially-flat Λ CDM model (Peebles 1984) with $\sim 70\%$ of the current cosmological energy budget being a time-independent cosmological constant (Λ), $\sim 25\%$ being non-relativistic cold dark matter (CDM), and most of the remaining $\sim 5\%$ being non-relativistic baryonic matter (see, e.g. Farooq et al. 2017; Scolnic et al. 2018; Planck Collaboration 2020; eBOSS Collaboration 2021). In this paper we also study cosmological models with a little spatial curvature or dynamical dark energy, since the observations do not rule out such models, and since some sets of measurements seem mutually incompatible when analyzed in the spatially-flat Λ CDM model (see, e.g. Di Valentino et al. 2021b; Perivolaropoulos & Skara 2021).

It is still unclear whether this incompatibility is evidence against the spatially-flat Λ CDM model or is caused by unidentified systematic errors in one of the established cosmological probes or by evolution of the parameters themselves with the redshift (Dainotti et al. 2021b, 2022). Newer, alternate cosmological probes could help alleviate this issue. Recent examples of such probes include reverberation-mapped quasar (QSO) measurements that reach to redshift $z \sim 1.9$ (Czerny et al. 2021; Zajaček et al. 2021; Yu et al. 2021; Khadka et al. 2021b,a), HII starburst galaxy measurements that reach to $z \sim 2.4$ (Mania & Ratra 2012; Chávez et al. 2014; González-Morán et al. 2019, 2021; Cao et al. 2020, 2022a, 2021a; Johnson et al. 2022; Mehrabi et al. 2022), QSO angular size measurements that reach to $z \sim 2.7$ (Cao et al. 2017; Ryan et al. 2019; Cao et al. 2020, 2021a; Zheng et al. 2021; Lian et al. 2021), QSO flux measurements that reach to $z \sim 7.5$ (Risaliti & Lusso 2015, 2019; Khadka & Ratra 2020a,b, 2021, 2022; Lusso et al. 2020; Yang et al. 2020; Zhao & Xia 2021; Li et al. 2021; Lian et al. 2021;

* E-mail: shulei@phys.ksu.edu

† E-mail: maria.dainotti@nao.ac.jp

‡ E-mail: ratra@phys.ksu.edu

Rezaei et al. 2021; Luongo et al. 2021),¹ and the main subject of this paper, gamma-ray burst (GRB) measurements that reach to $z \sim 8.2$ (Amati et al. 2008, 2019; Cardone et al. 2009, 2010; Samushia & Ratra 2010; Dainotti et al. 2013a,b; Postnikov et al. 2014; Wang et al. 2015, 2016, 2022; Fana Dirirsa et al. 2019; Khadka & Ratra 2020c; Hu et al. 2021; Dai et al. 2021; Demianski et al. 2021; Khadka et al. 2021c; Luongo et al. 2021; Luongo & Muccino 2021; Cao et al. 2021a)[Dainotti et al. 2011a,b, Apj, Mnras]. Some of these probes might eventually allow for a reliable extension of the Hubble diagram to $z \sim 3 - 4$, well beyond the reach of Type Ia supernovae. GRBs have been detected to $z \sim 9.4$ (Cucchiara et al. 2011), and might be detectable to $z = 20$ (Lamb & Reichart 2000), so in principle GRBs could act as a cosmological probe to higher redshifts than 8.2.

Cao et al. (2022b) recently used the A118 two-parameter Amati-correlated GRB data set (Khadka et al. 2021c) and the MD-LGRB, GW-LGRB, and MD-SGRB two-parameter Dainotti-correlated GRB data sets (Wang et al. 2022; Hu et al. 2021) to constrain cosmological parameters.² The circularity problem was circumvented by simultaneously constraining cosmological model parameters and GRB correlation parameters (see Dainotti et al. 2013b for a more extended discussion) and the cosmological-model-independence of the GRB correlation parameters shows that these GRBs are standardizable (Khadka & Ratra 2020c; Cao et al. 2022b). Not only does the simultaneous fitting method circumvent the circularity problem, it also allows for the derivation of unbiased GRB-only constraints (unlike the constraints derived from GRBs that have been calibrated by using other data, that are correlated with the calibrating data), that can be straightforwardly used to compare with other constraints derived from other data, such as $H(z) + \text{BAO}$ data as we have done here. The A118, MD-LGRB, GW-LGRB, and MD-SGRB GRBs provide cosmological constraints that are mostly compatible with those determined using better-established cosmological probes (Cao et al. 2022b).

Here, we use the new Platinum compilation of 50 long GRBs, spanning $0.553 \leq z \leq 5.0$, that obey the three-parameter fundamental plane (Dainotti) correlation between the peak prompt luminosity, the luminosity at the end of the plateau emission and its rest frame duration (Dainotti et al. 2016, 2017, 2020) to constrain cosmological model parameters and GRB correlation parameters. The platinum sample is listed in Table A1 of Appendix A. For this data set, measured quantities for a GRB are redshift z , characteristic time scale T_X^* , which marks the end of the plateau

¹ The most recent Lusso et al. (2020) QSO flux compilation assumes a UV–X-ray correlation model that is invalid above a significantly lower redshift, $z \sim 1.5 - 1.7$, so these QSOs can only be used to derive lower- z cosmological constraints (Khadka & Ratra 2021, 2022).

² The Amati correlation relates the rest-frame peak photon energy and the rest-frame isotropic radiated energy (Amati et al. 2008) and the two-dimensional Dainotti correlation relates the luminosity at the end of the plateau phase and the rest-frame end-time of plateau emission (Dainotti et al. 2008, 2010, 2011, 2013a, 2015, 2017). As discussed below, in this paper we use three-dimensional Dainotti and two-dimensional Amati correlation GRBs.

emission, the measured γ -ray energy flux F_X at T_X^* and the prompt peak flux F_{peak} over a 1 s interval, and X-ray spectral index of the plateau phase β' . This sample spans the redshift range $0.553 \leq z \leq 5.0$. We find that the Platinum GRBs are standardizable through the Dainotti correlation and they also provides cosmological parameter constraints compatible with those from better-established cosmological probes, as well as with those derived from A118 GRB data. We also combine the Platinum data set with the 101 non-overlapping Amati-correlated GRBs (A101) from the A118 data set to perform a joint (Platinum + A101) analysis. We find that this joint GRB data set provides slightly more restrictive cosmological constraints (in which the twice-as-large A101 data set dominates the statistics and so plays a more dominant role) that are consistent with those from a combined analysis of baryon acoustic oscillation (BAO) and Hubble parameter [$H(z)$] data. However, the cosmological constraints from Platinum, A118, A101, and Platinum + A101 data are less restrictive (precise) than those from $H(z) + \text{BAO}$ data because there are more parameters to be constrained in the GRB cases but not yet enough precise-enough data points to determine more precise GRB constraints. A joint analysis of the $H(z) + \text{BAO} + \text{Platinum} + \text{A101}$ data results in slightly more restrictive cosmological constraints relative to those from just $H(z) + \text{BAO}$ data.

Our paper is organized as follows. We summarize the cosmological models we use in Sec. 2 and outline the data sets adopted in Sec. 3. We then describe our analyses methods in Sec. 4 and discuss results in Sec. 5. We summarize our conclusions in Sec. 6.

2 COSMOLOGICAL MODELS

We constrain cosmological model parameters and GRB correlation parameters in six spatially-flat and non-flat dark energy cosmological models.³ The essential cosmological quantity for constraining purposes, for data we use, is the Hubble parameter, $H(z, \mathbf{p}) \equiv H_0 E(z, \mathbf{p})$, with H_0 being the Hubble constant and $E(z, \mathbf{p})$ the expansion rate as a function of redshift z and the cosmological parameters \mathbf{p} . Here we consider one massive and two massless neutrino species, with the effective number of relativistic neutrino species $N_{\text{eff}} = 3.046$ and the total neutrino mass $\sum m_\nu = 0.06$ eV. The non-relativistic neutrino physical energy density parameter is $\Omega_\nu h^2 = \sum m_\nu / (93.14 \text{ eV})$, where h is the reduced Hubble constant in units of $100 \text{ km s}^{-1} \text{ Mpc}^{-1}$. With the baryonic ($\Omega_b h^2$) and cold dark matter ($\Omega_c h^2$) physical energy density parameters as free cosmological parameters to be constrained, the derived non-relativistic matter density parameter is therefore $\Omega_m = (\Omega_\nu h^2 + \Omega_b h^2 + \Omega_c h^2)/h^2$.

In the flat and non-flat ΛCDM models, the expansion

³ For recent constraints on spatial curvature see Zhang et al. (2014), Chen et al. (2016), Rana et al. (2017), Ooba et al. (2018a,c), Yu et al. (2018), Park & Ratra (2019c,a), Wei (2018), DES Collaboration (2019), Li et al. (2020), Handley (2019), Efstathiou & Gratton (2020), Di Valentino et al. (2021a), Vagnozzi et al. (2021a,b), KiDS Collaboration (2021), Arjona & Nesseris (2021), Dhawan et al. (2021), Renzi et al. (2021), Geng et al. (2022), and references therein.

rate function

$$E(z) = \sqrt{\Omega_{m0}(1+z)^3 + \Omega_{k0}(1+z)^2 + \Omega_\Lambda}, \quad (1)$$

where $\Omega_\Lambda = 1 - \Omega_{m0} - \Omega_{k0}$ is the cosmological constant dark energy density parameter and Ω_{k0} is the curvature energy density parameter. In the non-flat Λ CDM model the free parameters being constrained are H_0 , $\Omega_b h^2$, $\Omega_c h^2$, and Ω_{k0} , whereas in the flat Λ CDM model $\Omega_{k0} = 0$ is implied.

In the flat and non-flat XCDM parametrizations,

$$E(z) = \sqrt{\Omega_{m0}(1+z)^3 + \Omega_{k0}(1+z)^2 + \Omega_X(1+z)^{3(1+w_X)}}, \quad (2)$$

where w_X and $\Omega_X = 1 - \Omega_{m0} - \Omega_{k0}$ are the equation of state parameter and the dynamical dark energy density parameter of the X-fluid, respectively. In the non-flat XCDM parameterization the free parameters being constrained are H_0 , $\Omega_b h^2$, $\Omega_c h^2$, Ω_{k0} , and w_X whereas in the flat XCDM parametrization $\Omega_{k0} = 0$ is implied.

In the flat and non-flat ϕ CDM models (Peebles & Ratra 1988; Ratra & Peebles 1988; Pavlov et al. 2013),⁴

$$E(z) = \sqrt{\Omega_{m0}(1+z)^3 + \Omega_{k0}(1+z)^2 + \Omega_\phi(z, \alpha)}, \quad (3)$$

where the scalar field, ϕ , dynamical dark energy density parameter

$$\Omega_\phi(z, \alpha) = \frac{1}{6H_0^2} \left[\frac{1}{2}\dot{\phi}^2 + V(\phi) \right], \quad (4)$$

and can be numerically computed by solving the Friedmann equation (3) and the equation of motion of the scalar field

$$\ddot{\phi} + 3H\dot{\phi} + V'(\phi) = 0. \quad (5)$$

We assume an inverse power-law scalar field potential energy density

$$V(\phi) = \frac{1}{2}\kappa m_p^2 \phi^{-\alpha}. \quad (6)$$

In these equations an overdot and a prime denote a derivative with respect to time and ϕ , respectively, m_p is the Planck mass, α is a positive constant, and the constant κ is determined by the shooting method in the Cosmic Linear Anisotropy Solving System (CLASS) code (Blas et al. 2011). In the non-flat ϕ CDM model the free parameters being constrained are H_0 , $\Omega_b h^2$, $\Omega_c h^2$, Ω_{k0} , and α , whereas in the flat ϕ CDM model $\Omega_{k0} = 0$ is implied.

3 DATA

In this paper we analyze two different GRB data sets as well as combinations of them and the joint $H(z) +$ BAO data set. These data sets are summarized in Table 1 and described below.⁵

⁴ For recent constraints on ϕ CDM see Chen et al. (2017), Zhai et al. (2017), Ooba et al. (2018b, 2019), Park & Ratra (2018, 2019b, 2020), Sangwan et al. (2018), Solà Peracaula et al. (2019), Singh et al. (2019), Ureña-López & Roy (2020), Sinha & Banerjee (2021), Xu et al. (2021), de Cruz Perez et al. (2021), Jesus et al. (2021), and references therein.

⁵ In this table and elsewhere, for compactness, we sometimes use Plat. as an abbreviation for the Platinum data set.

Table 1. Summary of data sets used.

Data set	N (Number of points)	Redshift range
Platinum	50	$0.553 \leq z \leq 5.0$
A118	118	$0.3399 \leq z \leq 8.2$
A101 ^a	101	$0.3399 \leq z \leq 8.2$
Plat. + A101	151	$0.3399 \leq z \leq 8.2$
$H(z)$	31	$0.070 \leq z \leq 1.965$
BAO	11	$0.38 \leq z \leq 2.334$

^a Excluding from A118 those GRBs in common with Platinum [060418, 080721, 081008, 090418(A), 091020, 091029, 110213(A), 110818(A), 111008(A), 120811C, 120922(A), 121128(A), 131030A, 131105A, 140206A, 150314A, and 150403A].

Platinum sample. This includes 50 long GRBs which exhibit a plateau phase with an angle $< 41^\circ$, that do not have a flare during the plateau, and have a plateau with duration longer than 500 s. The first criterion is based on evidence that the plateau angles are Gaussianly distributed and those with angle $> 41^\circ$ are outliers; the second criterion allows one to eliminate cases contaminated by the presence of flaring activity; and, the third criterion allows one to eliminate cases where prompt emission may mask the plateau to the point that the definition of the plateau is uncertain (Willingale et al. 2007, 2010). As discussed below, the Platinum GRBs obey the three-dimensional Dainotti relation. The platinum sample is listed in Table A1 of Appendix A. For this data set, measured quantities for a GRB are redshift z , characteristic time scale T_X^* , which marks the end of the plateau emission, the measured γ -ray energy flux F_X at T_X^* and the prompt peak flux F_{peak} over a 1 s interval, and X-ray spectral index of the plateau phase β' . This sample spans the redshift range $0.553 \leq z \leq 5.0$.

A118 sample. This sample include 118 long GRBs, listed in Table 7 of Khadka et al. (2021c), that obey the two-dimensional Amati relation. For this data set, measured quantities for a GRB are z , rest-frame spectral peak energy E_{p} , and measured bolometric fluence S_{bolo} , computed in the standard rest-frame energy band $1 - 10^4$ keV. This sample spans the redshift range $0.3399 \leq z \leq 8.2$.

A101 sample. The A118 data and the Platinum data have 17 common GRBs that are listed in the footnote of Table 1. We exclude these common GRBs from the A118 data set to form the A101 data set for joint analyses with the Platinum data set. This sample spans the redshift range $0.3399 \leq z \leq 8.2$.

Platinum + A101 sample. This combination GRB sample includes 151 GRBs. This sample spans the redshift range $0.3399 \leq z \leq 8.2$.

$H(z)$ and BAO data. There are 31 $H(z)$ and 11 BAO measurements that have a redshift range $0.07 \leq z \leq 1.965$ and $0.0106 \leq z \leq 2.33$, respectively. The $H(z)$ data are in Table 2 of Ryan et al. (2018) and the BAO data are in Table 1 of Cao et al. (2021b). We compare cosmological constraints from $H(z) +$ BAO data with those obtained from the GRB data sets, and also jointly analyze GRB and $H(z) +$ BAO data.

Table 2. Flat priors of the constrained parameters.

Parameter	Prior
Cosmological Parameters	
H_0^a	[None, None]
$\Omega_b h^2 b$	[0, 1]
$\Omega_c h^2 c$	[0, 1]
Ω_{k0}	[-2, 2]
α	[0, 10]
w_X	[-5, 0.33]
GRB Correlation Parameters	
a	[-5, 5]
b	[-5, 5]
C_o	[-50, 50]
σ_{int}	[0, 5]
β	[0, 5]
γ	[0, 300]

^a km s⁻¹ Mpc⁻¹. In all four GRB-only analyses, H_0 is set to be 70 km s⁻¹ Mpc⁻¹, while in other cases the prior range is irrelevant (unbounded).

^b In all four GRB-only analyses, $\Omega_b h^2$ is set to be 0.0245, i.e. $\Omega_b = 0.05$.

^c In all four GRB-only analyses, the Ω_c range is adjusted to ensure $\Omega_{m0} \in [0, 1]$.

4 DATA ANALYSIS METHODOLOGY

Luminosity distance, D_L , as a function of z and cosmological parameters \mathbf{p} , is given by

$$D_L(z, \mathbf{p}) = \begin{cases} \frac{c(1+z)}{H_0 \sqrt{|\Omega_{k0}|}} \sinh \left[\frac{\sqrt{|\Omega_{k0}|} H_0}{c} D_C(z, \mathbf{p}) \right] & \text{if } \Omega_{k0} > 0, \\ (1+z) D_C(z, \mathbf{p}) & \text{if } \Omega_{k0} = 0, \\ \frac{c(1+z)}{H_0 \sqrt{|\Omega_{k0}|}} \sin \left[\frac{H_0 \sqrt{|\Omega_{k0}|}}{c} D_C(z, \mathbf{p}) \right] & \text{if } \Omega_{k0} < 0, \end{cases} \quad (7)$$

where the comoving distance is

$$D_C(z, \mathbf{p}) = c \int_0^z \frac{dz'}{H(z', \mathbf{p})}, \quad (8)$$

c is the speed of light, and $H(z, \mathbf{p})$ is the Hubble parameter that is described in Sec. 2 for each cosmological model.

For Platinum GRBs the X-ray source rest-frame luminosity L_X , time T_X^* at the end of the plateau emission, and the peak prompt luminosity L_{peak} are correlated through the three-parameter fundamental plane relation (Dainotti et al. 2016, 2017, 2020, 2021a)

$$\log L_X = C_o + a \log T_X^* + b \log L_{\text{peak}}, \quad (9)$$

where

$$L_X = \frac{4\pi D_L^2}{(1+z)^{1-\beta'}} F_X, \quad (10)$$

$$L_{\text{peak}} = \frac{4\pi D_L^2}{(1+z)^{1-\beta'}} F_{\text{peak}}, \quad (11)$$

C_o is the intercept parameter, and a and b are the slope parameters, with all three to be determined from data. F_X and F_{peak} are the measured γ -ray energy flux (erg cm⁻² s⁻¹) at T_X^* and in the peak of the prompt emission over a

1 s interval, respectively, and β' is the X-ray spectral index of the plateau phase.

We compute L_X and L_{peak} as functions of cosmological parameters \mathbf{p} at the redshift of each GRB by using eqs. (7), (10), and (11). We then compute the natural log of the likelihood function (D'Agostini 2005)

$$\ln \mathcal{L}_{\text{GRB}} = -\frac{1}{2} \left[\chi_{\text{GRB}}^2 + \sum_{i=1}^N \ln (2\pi\sigma_{\text{tot},i}^2) \right], \quad (12)$$

where

$$\chi_{\text{GRB}}^2 = \sum_{i=1}^N \left[\frac{(\log L_{X,i} - C_o - a \log T_{X,i}^* - b \log L_{\text{peak},i})^2}{\sigma_{\text{tot},i}^2} \right], \quad (13)$$

with

$$\sigma_{\text{tot},i}^2 = \sigma_{\text{int},P}^2 + \sigma_{\log L_{X,i}}^2 + a^2 \sigma_{\log T_{X,i}^*}^2 + b^2 \sigma_{\log L_{\text{peak},i}}^2. \quad (14)$$

where $\sigma_{\text{int},P}$ is the Platinum GRB data intrinsic scatter parameter, that also contains the unknown systematic uncertainty, and N is the number of data points.

For GRBs which obey the Amati correlation, a detailed description of the procedure can be found in Sec. 4 of Cao et al. (2022b). Here we denote its intrinsic scatter parameter as $\sigma_{\text{int,A}}$ as opposed to the Platinum one, $\sigma_{\text{int},P}$.

Detailed descriptions of the $H(z) + \text{BAO}$ data analysis procedure can be found in Sec. 4 of Cao et al. (2020) and Cao et al. (2021b).

The flat priors of the free parameters are listed in Table 2. The best-fitting values and posterior distributions of all free parameters are obtained through maximizing the likelihood functions using the Markov chain Monte Carlo (MCMC) code MONTEPYTHON (Brinckmann & Lesgourges 2019), with the physics coded in CLASS. The convergence of the MCMC chains for each free parameter is guaranteed by the Gelman-Rubin criterion ($R - 1 < 0.05$). The PYTHON package GETDIST (Lewis 2019) is used to compute the posterior means and uncertainties and plot the marginalized likelihood distributions and contours.

We use the Akaike Information Criterion (AIC) and the Bayesian Information Criterion (BIC) to compare the goodness of fit of models with different numbers of parameters. Their definitions can be found in Cao et al. (2022b). We also compare the goodness of fit using the DIC criterion (Kunz et al. 2006; Amati et al. 2019) defined as

$$DIC = -2 \ln \mathcal{L}_{\max} + 2n_{\text{eff}}, \quad (15)$$

where $n_{\text{eff}} = \langle -2 \ln \mathcal{L} \rangle + 2 \ln \mathcal{L}_{\max}$ is the number of effectively constrained parameters with brackets representing the average over the posterior distribution. We compute ΔAIC , ΔBIC , and ΔDIC differences of the other five cosmological models with respect to the flat Λ CDM reference model. Positive (negative) values of ΔAIC , ΔBIC , or ΔDIC indicate that the model under study fits the data worse (better) than does the reference model. Relative to the model with minimum $AIC(BIC/DIC)$, $\Delta AIC(BIC/DIC) \in (0, 2]$ is said to be weak evidence against the candidate model, $\Delta AIC(BIC/DIC) \in (2, 6]$ is positive evidence against the candidate model, while $\Delta AIC(BIC/DIC) \in (6, 10]$ is strong evidence against the candidate model, with $\Delta AIC(BIC/DIC) > 10$ being very strong evidence against the candidate model.

5 RESULTS

We show the posterior one-dimensional (1D) probability distributions and two-dimensional (2D) confidence regions of cosmological-model and GRB-correlation parameters for the six cosmological models in Figs. 1–7, in gray (Platinum), green (A118 and A101), orange (Platinum + A101), red [$H(z)$ + BAO], and blue [$H(z)$ + BAO + Platinum, in short HzBP, and $H(z)$ + BAO + Platinum + A101, in short HzBPA101]. The unmarginalized best-fitting parameter values, as well as the values of maximum likelihood \mathcal{L}_{\max} , AIC , BIC , DIC , ΔAIC , ΔBIC , and ΔDIC , for all models and data combinations, are listed in Table 3. We list the marginalized posterior mean parameter values and uncertainties ($\pm 1\sigma$ error bars and 1 or 2σ limits), for all models and data combinations, in Table 4.

5.1 Constraints from Platinum, A118, A101, and Platinum + A101 data

As in Khadka et al. (2021c) and Cao et al. (2022b), in the four GRB-only cases here we set $H_0 = 70 \text{ km s}^{-1} \text{ Mpc}^{-1}$ and $\Omega_b = 0.05$.

The constraints on the Platinum GRB correlation parameters in the six different cosmological models are mutually consistent, so the three-dimensional Dainotti correlation Platinum data set is standardizable. The constraints on the intrinsic scatter parameter $\sigma_{\text{int}, p}$ are almost identical, ranging from $0.346^{+0.032}_{-0.044}$ (flat ϕ CDM) to $0.347^{+0.034}_{-0.046}$ (non-flat Λ CDM). The constraints on the slope a range from a low of -0.727 ± 0.109 (non-flat Λ CDM and non-flat XCDM) to a high of -0.714 ± 0.104 (flat Λ CDM), the constraints on the slope b range from a low of $0.736^{+0.102}_{-0.087}$ (non-flat XCDM) to a high of 0.756 ± 0.083 (flat Λ CDM), and the constraints on the intercept C_o range from a low of 11.52 ± 4.45 (flat Λ CDM) to a high of $12.62^{+4.65}_{-5.51}$ (non-flat XCDM), with central values of each pair being 0.09σ , 0.15σ , and 0.16σ away from each other, respectively. We note that a compilation of (the two-parameter) Dainotti-correlation GRBs, the 31 MD-LGRBs of Wang et al. (2022), have a somewhat smaller intrinsic dispersion, $\sigma_{\text{int}} \sim 0.303 - 0.306$, Table 5 of Cao et al. (2022b), than the $\sigma_{\text{int}, p} \sim 0.346 - 0.347$ of the 50 Platinum GRBs.⁶ A possible reason for the smaller scatter of the 2-parameter MD-LGRB sample is due to how the sample was chosen. In principle one can retain fewer GRBs that lie exactly on the plane, or are much closer to the plane, thus reducing the scatter. However, further investigation is needed in order to draw a definite conclusion. Probably as a consequence of the smaller σ_{int} , the MD-LGRB constraints on Ω_{m0} and Ω_{k0} are more restrictive than the constraints from Platinum data.

⁶ There are 12 common GRBs between the Platinum and MD-LGRB data sets (060605, 060906, 061222A, 070306, 080310, 081008, 120404A, 160121A, 160227A, 180329B, 190106A, and 190114A). There are also common GRBs between the Platinum and the (two-parameter) Dainotti-correlated GW-LGRB compilation of Hu et al. (2021) [091029, 120118B, 131105A, 170202A, 170705A, and 151027A (same name but different redshifts)]. Because of the significant number of overlapping GRBs in these cases, we believe it would not be that useful to perform joint analyses of the Platinum and truncated (to remove the overlapping GRBs) MD-LGRB or GW-LGRB data sets.

Compared with the analyses in Cao et al. (2022b) where we neglect massive neutrinos (setting $\Omega_\nu h^2 = 0$), here we include a non-zero $\Omega_\nu h^2$. The constraints on the A118 GRB correlation parameters here are almost identical to those listed in Table 8 of Cao et al. (2022b) and are cosmological-model-independent implying that the A118 GRBs are standardizable. For the 118 GRBs A118 data $\sigma_{\text{int}, A} \sim 0.411 - 0.412$, larger than the $\sigma_{\text{int}, P} \sim 0.346 - 0.347$ of the 50 Platinum GRBs. The constraints on the A101 GRB correlation parameters are also cosmological-model-independent, so A101 GRBs are also standardizable. The constraints on the A101 intrinsic scatter parameter $\sigma_{\text{int}, A}$ range from a low of $0.419^{+0.030}_{-0.037}$ (non-flat Λ CDM) to a high of $0.422^{+0.030}_{-0.037}$ (flat Λ CDM and flat XCDM), which are slightly (0.2σ at most) higher than those from A118 data; the constraints on the slope β range from a low of 1.140 ± 0.098 (flat Λ CDM) to a high of 1.157 ± 0.098 (non-flat XCDM), which are slightly (0.28σ at most) higher than those from A118 data; and the constraints on the intercept γ range from a low of 49.91 ± 0.30 (non-flat XCDM) to a high of $50.10^{+0.29}_{-0.33}$ (flat XCDM), which are slightly (0.25σ at most) lower than those from A118 data; with central values of each pair being 0.06σ , 0.12σ , and 0.43σ away from each other, respectively.

Below we discuss cosmological parameter constraints in more detail. From Fig. 7 we see that the overlap of the constraints on the cosmological parameters indicate that Platinum data and A101 data cosmological constraints are mutually consistent and so these two data sets can be jointly analyzed. The Platinum + A101 data combination is also standardizable with cosmological-model-independent constraints on GRB correlation parameters that are consistent (well within 1σ) with those from both Platinum data and A101 data individually.

We find that in the flat Λ CDM model and the flat XCDM parametrization all GRB data more favor currently accelerating cosmological expansion. In the non-flat Λ CDM model, all but the Platinum GRBs more favor currently decelerating cosmological expansion. In the non-flat XCDM parametrization, in the $\Omega_{k0} - \Omega_{m0}$ parameter subspace, all but the Platinum GRBs more favor currently decelerating cosmological expansion, while in the $w_X - \Omega_{m0}$ ($w_X - \Omega_{k0}$) parameter subspace, all (all but the A101) GRBs more favor currently accelerating cosmological expansion. In the flat and non-flat ϕ CDM models, currently decelerating cosmological expansion is slightly more favored.

Cosmological constraints from Platinum data are less restrictive than those from A118 and A101 data, which contain a little more than twice as many GRBs than the Platinum compilation. Comparing the Platinum + A101 constraints with the Platinum constraints and with the A101 constraints, we see that A101 data, with double the number of GRBs compared to Platinum, play a more dominant role in the combination.

In the flat and non-flat Λ CDM models, the Platinum, A118, A101, and Platinum + A101 2σ constraints on Ω_{m0} are mutually consistent and also consistent with those of $H(z)$ + BAO, with the 2σ lower limits in the flat (non-flat) Λ CDM model being None (None), > 0.256 (> 0.295), > 0.191 (> 0.212), and > 0.216 (> 0.235), respectively. In the flat Λ CDM model, the A101 constraint on Ω_{m0} is more consistent (than the Platinum and Platinum + A101 constraints) with that from $H(z)$ + BAO data, differing by

Table 3: Unmarginalized best-fitting parameter values for all models from various combinations of data.

Model	Data set	$\Omega_b h^2$ ^a	$\Omega_c h^2$	$\Omega_{\text{m}0}$	$\Omega_{\text{r}0}$	w_{X}/a ^b	H_0^c	$\sigma_{\text{int}, \text{P}}$	a	b	C_o	$\sigma_{\text{int}, \text{A}}$	γ	β	$-2 \ln \mathcal{L}_{\text{max}}$	AIC	BIC	DIC	ΔAIC	ΔBIC	ΔDIC	
Flat	Platinum	—	0.4560	0.982	—	—	0.322	-0.716	0.743	12.19	—	—	—	—	32.99	42.99	52.55	42.80	0.00	0.00	0.00	
	A118	—	0.4088	0.886	—	—	—	—	—	—	—	—	—	—	128.72	136.72	147.81	136.05	0.00	0.00	0.00	
	A101	—	0.2547	0.571	—	—	—	—	—	—	—	—	—	—	112.81	120.81	131.27	120.16	0.00	0.00	0.00	
	Plat. + A101	—	0.3505	0.767	—	—	0.324	-0.694	0.753	11.60	0.413	49.98	1.125	—	146.08	162.08	186.22	162.07	0.00	0.00	0.00	
	$H(z) + \text{BAO}$	0.0240	0.1177	0.298	—	—	69.11	—	—	—	—	—	—	—	23.66	29.66	34.87	30.23	0.00	0.00	0.00	
	HzBP ^d	0.0243	0.1169	0.298	—	—	69.04	0.325	-0.715	0.757	11.53	—	—	—	57.33	73.33	88.99	72.58	0.00	0.00	0.00	
Non-flat	Plat. + A101	—	0.1155	0.296	—	—	68.71	0.324	-0.707	0.760	11.35	0.412	50.16	1.153	170.63	190.63	223.26	191.94	0.00	0.00	0.00	
	Platinum	—	0.1178	0.292	-0.992	—	—	0.292	-0.700	0.829	7.59	—	—	—	24.51	36.51	47.98	51.00	-6.48	-4.57	8.20	
	A118	—	0.4625	0.995	1.094	—	—	—	—	—	—	—	—	—	127.96	137.96	151.82	136.72	1.24	4.01	0.67	
	A101	—	0.4606	0.991	1.093	—	—	—	—	—	—	—	—	—	111.08	121.08	134.16	120.04	0.27	2.89	-0.12	
	Plat. + A101	—	0.4300	0.929	1.857	—	—	0.326	-0.712	0.746	11.99	0.400	49.75	1.167	144.65	162.65	189.80	161.75	0.57	3.58	-0.32	
	$H(z) + \text{BAO}$	0.0247	0.1141	0.295	0.023	—	68.78	—	—	—	—	—	—	—	23.59	31.59	38.54	32.21	1.93	3.67	1.99	
Non-flat	Plat. + A101	—	0.0245	0.1149	0.294	0.010	—	68.99	0.328	-0.719	0.752	11.81	—	—	—	57.31	73.31	93.48	74.65	-0.02	4.49	2.07
	Platinum	—	0.1115	0.295	0.032	—	67.91	0.328	-0.726	0.750	11.91	0.410	50.13	1.164	170.70	192.70	228.59	193.50	2.07	5.33	1.56	
	A118	—	0.0809	0.216	—	0.137	—	0.323	-0.724	0.735	12.59	—	—	—	32.81	44.81	56.28	42.83	1.82	3.73	0.04	
	A101	—	-0.0198	0.011	—	-0.139	—	—	—	—	—	—	—	—	128.42	138.42	152.28	136.65	1.70	4.47	0.61	
	Plat. + A101	—	-0.0221	0.006	—	-0.251	—	—	—	—	—	—	—	—	111.99	121.99	135.06	121.23	1.18	3.79	0.08	
	$H(z) + \text{BAO}$	0.0309	0.0870	0.280	—	-0.1570	0.372	—	-0.193	0.317	-0.712	0.753	11.65	0.405	50.02	1.115	145.74	163.74	190.90	162.40	1.66	4.68
Non-flat	Plat. + A101	—	0.0302	0.0899	0.284	—	65.11	—	—	—	—	—	—	—	19.65	27.65	34.60	28.11	-2.01	-0.27	-2.11	
	Platinum	—	0.0918	0.239	-0.760	-1.123	—	0.286	-0.761	0.788	10.04	—	—	—	24.58	38.58	51.97	51.01	-4.41	-0.58	8.21	
	A118	—	0.4644	0.999	0.998	-1.137	—	—	—	—	—	—	—	—	127.97	139.97	156.60	137.16	3.25	8.79	1.11	
	A101	—	0.4444	0.958	1.849	-1.222	—	—	—	—	—	—	—	—	111.14	123.14	138.83	120.59	2.33	7.56	0.44	
	Plat. + A101	—	0.4120	0.892	1.526	-1.208	—	0.335	-0.707	0.758	11.34	0.405	49.77	1.163	144.69	164.69	194.86	162.75	2.61	8.64	0.67	
	$H(z) + \text{BAO}$	0.0295	0.0962	0.294	-0.159	-0.648	65.62	—	—	—	—	—	—	—	18.31	37.00	37.00	37.00	-1.35	2.13	-1.26	
Non-flat	Plat. + A101	—	0.0301	0.0933	0.290	-0.164	-0.640	65.39	0.324	-0.709	0.746	12.04	—	—	—	51.90	69.90	92.60	70.74	-3.43	3.61	-1.85
	Platinum	—	0.0883	0.284	-0.112	-0.640	64.65	0.319	-0.714	0.767	11.01	0.414	50.19	1.137	165.30	189.30	228.45	189.85	-1.33	5.19	-2.09	
	A118	—	0.4615	0.993	—	4.896	-1.137	—	—	—	—	—	—	—	32.99	44.99	56.46	42.37	2.00	3.91	-0.43	
	A101	—	0.2119	0.484	—	9.617	—	—	—	—	—	—	—	—	128.56	138.56	152.41	135.74	1.84	4.60	-0.31	
	Plat. + A101	—	0.0764	0.207	—	9.922	—	—	—	—	—	—	—	—	112.26	122.26	135.33	119.96	1.45	4.06	-0.20	
	$H(z) + \text{BAO}$	0.0332	0.0936	0.242	—	7.330	—	0.326	-0.723	0.755	11.62	0.410	50.04	1.135	145.75	163.75	190.90	161.62	1.67	4.68	-0.46	
Non-flat	Plat. + A101	—	0.0343	0.0789	0.265	—	1.455	65.24	—	—	—	—	—	—	19.49	27.49	34.44	26.96	-2.17	-0.43	-3.27	
	Platinum	—	0.0374	0.0663	0.246	—	1.633	64.98	0.331	-0.714	0.765	11.10	—	—	—	53.12	69.12	89.29	69.20	-4.21	0.30	-3.39
	A118	—	0.4366	0.942	-0.905	0.061	—	0.325	-0.735	0.744	12.14	—	—	—	32.53	46.53	59.92	43.06	3.54	7.37	0.26	
	A101	—	0.3331	0.731	0.234	5.269	—	—	—	—	—	—	—	—	128.42	140.42	157.04	136.67	3.70	9.23	0.63	
	Plat. + A101	—	0.2367	0.534	0.460	8.680	—	—	—	—	—	—	—	—	111.89	123.89	139.58	120.48	3.08	8.31	0.33	
	$H(z) + \text{BAO}$	0.0344	0.3063	0.677	0.317	9.746	—	0.319	-0.728	0.742	12.27	0.412	49.96	1.140	145.40	165.40	195.57	162.44	3.32	9.35	0.36	
Non-flat	Plat. + A101	—	0.0326	0.0786	0.263	-0.149	2.014	65.71	—	—	—	—	—	—	18.15	28.15	36.84	27.39	-1.51	1.97	-2.84	
	Platinum	—	0.0353	0.0730	0.257	-0.135	2.199	65.09	0.321	-0.729	0.758	11.52	0.403	50.16	1.144	165.08	189.08	228.23	188.65	-1.55	3.50	-3.14
	A118	—	0.3331	0.731	0.234	5.269	—	—	—	—	—	—	—	—	128.42	140.42	157.04	136.67	3.70	9.23	0.63	
	A101	—	0.2367	0.534	0.460	8.680	—	—	—	—	—	—	—	—	111.89	123.89	139.58	120.48	3.08	8.31	0.33	
	Plat. + A101	—	0.3063	0.677	0.317	9.746	—	0.319	-0.728	0.742	12.27	0.412	49.96	1.140	145.40	165.40	195.57	162.44	3.32	9.35	0.36	
	$H(z) + \text{BAO}$	0.0344	0.0786	0.263	-0.149	2.014	65.71	—	—	—	—	—	—	—	51.79	69.79	92.49	69.44	-3.54	3.50	-3.14	
Non-flat	Plat. + A101	—	0.0353	0.0730	0.257	-0.135	2.199	65.09	0.321	-0.729	0.758	11.52	0.403	50.16	1.144	165.08	189.08	228.23	188.65	-1.55	4.97	-3.29

^a In the four GRB-only cases $\Omega_b h^2$ is set to 0.0245.^b w_{X} corresponds to flat/non-flat XCDM and a corresponds to flat/non-flat ϕ CDM.^c $\text{km s}^{-1} \text{Mpc}^{-1}$. In the four GRB-only cases H_0 is set to 70 $\text{km s}^{-1} \text{Mpc}^{-1}$.^d $H(z) + \text{BAO} + \text{Platinum}$.^e $H(z) + \text{BAO} + \text{Platinum} + \text{A101}$.

Table 4: One-dimensional marginalized posterior mean values and uncertainties ($\pm 1\sigma$ error bars or 2σ limits) of the parameters for all models from various combinations of data.

Model	Data set	$\Omega_b h^2$ ^a	$\Omega_c h^2$	Ω_{m0}	Ω_{k0}	w_X/α ^b	H_0 ^c	$\sigma_{\text{int, p}}$	a	b	C_o	$\sigma_{\text{int, A}}$	γ	β	
Platinum	—	—	—	$> 0.411^{\text{d}}$	—	—	—	$0.347^{+0.036}_{-0.046}$	-0.714 ± 0.104	0.756 ± 0.083	11.52 ± 4.45	—	—	—	
A118	—	—	—	> 0.256	—	—	—	—	—	—	—	$0.412^{+0.027}_{-0.033}$	50.09 ± 0.25	1.109 ± 0.089	
A101	—	—	—	$0.584^{+0.248}_{-0.240}$	—	—	—	$0.347^{+0.033}_{-0.046}$	-0.717 ± 0.102	0.751 ± 0.083	11.80 ± 4.45	$0.422^{+0.028}_{-0.037}$	50.03 ± 0.28	1.140 ± 0.098	
Flat	Plat. + A101	0.0243 ± 0.0029	$0.1184^{+0.0077}_{-0.0084}$	$0.1184^{+0.0077}_{-0.0084}$	—	—	69.27 ± 1.85	—	—	—	—	$0.421^{+0.029}_{-0.036}$	50.03 ± 0.27	1.138 ± 0.095	
Λ CDM	$H(z)$ + BAO	0.0242 ± 0.0029	$0.1184^{+0.0076}_{-0.0084}$	$0.1184^{+0.0076}_{-0.0084}$	—	—	69.24 ± 1.81	$0.347^{+0.033}_{-0.046}$	-0.711 ± 0.104	0.762 ± 0.081	11.23 ± 4.35	—	—	—	
	HzBP ^e	$0.0242^{+0.0027}_{-0.0030}$	$0.1187^{+0.0075}_{-0.0083}$	$0.1187^{+0.0075}_{-0.0083}$	—	—	69.20 ± 1.79	$0.347^{+0.032}_{-0.045}$	-0.711 ± 0.104	0.762 ± 0.080	11.23 ± 4.32	$0.421^{+0.029}_{-0.036}$	50.13 ± 0.26	1.159 ± 0.094	
	HzBPA101 ^f	$0.0242^{+0.0027}_{-0.0030}$	$0.1187^{+0.0075}_{-0.0083}$	$0.1187^{+0.0075}_{-0.0083}$	—	—	—	—	—	—	—	—	—	—	
Platinum	—	—	—	$> 0.491^{\text{d}}$	$-0.023^{+0.869}_{-1.401}$	—	—	$0.347^{+0.034}_{-0.046}$	-0.727 ± 0.109	$0.738^{+0.102}_{-0.088}$	$12.49^{+4.71}_{-5.46}$	—	—	—	
A118	—	—	—	> 0.295	$0.701^{+0.636}_{-0.844}$	—	—	—	—	—	—	$0.411^{+0.027}_{-0.033}$	50.00 ± 0.26	1.123 ± 0.088	
A101	—	—	—	> 0.212	$0.886^{+0.519}_{-0.849}$	—	—	—	—	—	—	$0.419^{+0.027}_{-0.036}$	49.93 ± 0.27	1.156 ± 0.096	
Non-flat	Plat. + A101	$0.0255^{+0.0040}_{-0.0048}$	0.1127 ± 0.0195	0.293 ± 0.025	—	—	$0.346^{+0.031}_{-0.044}$	-0.711 ± 0.100	0.759 ± 0.080	$11.33^{+4.28}_{-4.27}$	—	—	—	1.154 ± 0.095	
Λ CDM	$H(z)$ + BAO	$0.0253^{+0.0048}_{-0.0049}$	$0.1135^{+0.0192}_{-0.0193}$	0.294 ± 0.024	—	—	68.76 ± 2.36	—	—	—	—	—	—	—	
	HzBP ^e	$0.0253^{+0.0048}_{-0.0049}$	$0.1135^{+0.0192}_{-0.0193}$	0.294 ± 0.024	—	—	68.80 ± 2.32	$0.347^{+0.033}_{-0.046}$	-0.710 ± 0.104	0.763 ± 0.080	11.18 ± 4.30	—	—	—	
	HzBPA101 ^f	$0.0255^{+0.0047}_{-0.0047}$	$0.1121^{+0.0182}_{-0.0182}$	0.293 ± 0.023	$0.043^{+0.094}_{-0.077}$	—	68.62 ± 2.24	$0.347^{+0.033}_{-0.046}$	-0.710 ± 0.102	0.764 ± 0.079	11.15 ± 4.27	$0.421^{+0.029}_{-0.036}$	50.13 ± 0.26	1.161 ± 0.093	
Platinum	—	—	—	$> 0.386^{\text{d}}$	—	< -0.078	—	$0.347^{+0.033}_{-0.046}$	-0.717 ± 0.103	0.749 ± 0.083	11.90 ± 4.45	—	—	—	
A118	—	—	—	$0.539^{+0.360}_{-0.166}$	—	$-2.412^{+1.790}_{-1.730}$	—	—	—	—	—	$0.412^{+0.028}_{-0.034}$	$50.15^{+0.27}_{-0.30}$	1.106 ± 0.090	
A101	—	—	—	$0.558^{+0.285}_{-0.280}$	—	$-2.423^{+1.765}_{-1.716}$	—	—	—	—	—	$0.422^{+0.037}_{-0.037}$	$50.10^{+0.29}_{-0.30}$	1.134 ± 0.097	
Flat	Plat. + A101	$0.0239^{+0.0046}_{-0.0052}$	$0.0026^{+0.0192}_{-0.0170}$	$0.283^{+0.023}_{-0.023}$	< 0.089	—	$0.346^{+0.033}_{-0.046}$	-0.718 ± 0.105	0.749 ± 0.084	11.94 ± 4.54	—	—	—	1.133 ± 0.094	
Λ CDM	$H(z)$ + BAO	$0.0301^{+0.0196}_{-0.0196}$	$0.0917^{+0.0196}_{-0.0196}$	$0.283^{+0.023}_{-0.023}$	—	$-0.750^{+0.149}_{-0.149}$	$63.83^{+2.34}_{-2.33}$	—	—	—	—	—	—	—	
	HzBP ^e	$0.0301^{+0.0196}_{-0.0196}$	$0.0917^{+0.0196}_{-0.0196}$	$0.283^{+0.023}_{-0.023}$	—	$-0.743^{+0.153}_{-0.150}$	$65.73^{+2.31}_{-2.33}$	$0.347^{+0.033}_{-0.046}$	-0.711 ± 0.104	0.763 ± 0.081	11.24 ± 4.32	—	—	—	
	HzBPA101 ^f	$0.0303^{+0.0196}_{-0.0196}$	$0.0904^{+0.0196}_{-0.0196}$	$0.282^{+0.023}_{-0.021}$	—	$-0.731^{+0.160}_{-0.166}$	$65.54^{+2.36}_{-2.58}$	$0.347^{+0.032}_{-0.046}$	-0.711 ± 0.102	0.762 ± 0.080	11.21 ± 4.38	$0.420^{+0.029}_{-0.036}$	50.14 ± 0.26	1.159 ± 0.093	
Platinum	—	—	—	$> 0.457^{\text{d}}$	$0.011^{+0.821}_{-1.155}$	$-2.212^{+1.779}_{-1.779}$	—	$0.346^{+0.034}_{-0.046}$	-0.727 ± 0.109	$0.736^{+0.102}_{-0.087}$	$12.62^{+4.65}_{-5.51}$	—	—	—	
A118	—	—	—	> 0.257	$0.569^{+0.174}_{-0.174}$	$-2.289^{+1.998}_{-1.988}$	—	—	—	—	—	$0.412^{+0.027}_{-0.033}$	50.01 ± 0.27	1.120 ± 0.088	
A101	—	—	—	> 0.193	$0.824^{+0.644}_{-0.644}$	$-2.338^{+1.938}_{-1.938}$	—	—	—	—	—	$0.421^{+0.033}_{-0.037}$	49.91 ± 0.30	1.157 ± 0.098	
Non-flat	Plat. + A101	$0.0291^{+0.0055}_{-0.0055}$	$0.0986^{+0.0218}_{-0.0218}$	0.294 ± 0.028	—	$-0.116^{+0.135}_{-0.135}$	$-0.702^{+0.139}_{-0.139}$	$63.98^{+2.36}_{-2.36}$	—	0.759 ± 0.081	$11.33^{+4.38}_{-4.34}$	—	—	—	1.154 ± 0.096
Λ CDM	$H(z)$ + BAO	$0.0292^{+0.0053}_{-0.0053}$	$0.0983^{+0.0218}_{-0.0218}$	0.294 ± 0.028	—	$-0.128^{+0.134}_{-0.134}$	$-0.695^{+0.141}_{-0.141}$	$65.93^{+2.33}_{-2.33}$	$0.347^{+0.033}_{-0.046}$	-0.713 ± 0.103	0.758 ± 0.082	11.46 ± 4.44	—	—	
	HzBP ^e	$0.0292^{+0.0053}_{-0.0053}$	$0.0948^{+0.0214}_{-0.0214}$	0.290 ± 0.027	-0.106 ± 0.128	$-0.690^{+0.144}_{-0.145}$	$65.65^{+2.34}_{-2.33}$	$0.346^{+0.033}_{-0.045}$	-0.713 ± 0.103	0.758 ± 0.081	11.44 ± 4.38	$0.421^{+0.029}_{-0.036}$	50.14 ± 0.26	1.151 ± 0.094	
Platinum	—	—	—	$> 0.379^{\text{d}}$	—	—	—	$0.346^{+0.032}_{-0.044}$	-0.715 ± 0.102	0.753 ± 0.081	11.68 ± 4.33	—	—	—	
A118	—	—	—	$0.576^{+0.355}_{-0.292}$	—	—	—	—	—	—	—	$0.411^{+0.027}_{-0.033}$	50.05 ± 0.25	1.110 ± 0.089	
A101	—	—	—	$0.506^{+0.292}_{-0.292}$	—	—	—	—	—	—	—	$0.421^{+0.037}_{-0.037}$	49.99 ± 0.27	1.140 ± 0.097	
Flat	Plat. + A101	$-$	$0.541^{+0.301}_{-0.297}$	—	—	$1.497^{+0.623}_{-0.623}$	65.12 ± 2.18	—	0.716 ± 0.103	0.751 ± 0.082	11.77 ± 4.39	$0.420^{+0.029}_{-0.036}$	49.99 ± 0.26	1.137 ± 0.095	
ϕ CDM	$H(z)$ + BAO	$0.0324^{+0.0060}_{-0.0060}$	$0.0809^{+0.0180}_{-0.0178}$	0.268 ± 0.024	—	$1.477^{+0.630}_{-0.630}$	$65.15^{+2.13}_{-2.13}$	$0.347^{+0.033}_{-0.045}$	-0.711 ± 0.104	0.762 ± 0.081	11.24 ± 4.37	—	—	—	
	HzBP ^e	$0.0325^{+0.0060}_{-0.0060}$	$0.0805^{+0.0178}_{-0.0177}$	0.267 ± 0.024	—	$1.509^{+0.630}_{-0.630}$	$65.03^{+2.10}_{-2.30}$	$0.347^{+0.033}_{-0.046}$	-0.711 ± 0.103	0.762 ± 0.082	$11.23^{+4.39}_{-4.38}$	$0.420^{+0.029}_{-0.036}$	50.14 ± 0.26	1.158 ± 0.093	
	HzBPA101 ^f	$0.0328^{+0.0060}_{-0.0060}$	$0.0794^{+0.0179}_{-0.0198}$	0.266 ± 0.025	—	$1.568^{+0.632}_{-0.911}$	$65.53^{+2.30}_{-2.29}$	$0.346^{+0.033}_{-0.046}$	-0.717 ± 0.105	0.751 ± 0.084	$11.78^{+4.51}_{-4.52}$	—	—	—	
Platinum	—	—	—	$0.537^{+0.427}_{-0.391}$	—	$-0.026^{+0.384}_{-0.384}$	—	—	—	—	—	$0.412^{+0.027}_{-0.033}$	50.05 ± 0.25	1.110 ± 0.090	
A118	—	—	—	$0.559^{+0.258}_{-0.258}$	—	$-0.002^{+0.300}_{-0.302}$	$5.185^{+3.757}_{-3.757}$	—	—	—	—	$0.421^{+0.037}_{-0.037}$	49.99 ± 0.27	1.146 ± 0.098	
A101	—	—	—	$0.507^{+0.256}_{-0.256}$	—	$0.107^{+0.266}_{-0.266}$	$5.205^{+3.944}_{-2.507}$	—	—	—	—	$0.421^{+0.037}_{-0.037}$	49.98 ± 0.26	1.142 ± 0.097	
Non-flat	Plat. + A101	$0.5320^{+0.0060}_{-0.0060}$	$0.0847^{+0.0179}_{-0.0178}$	0.272 ± 0.028	—	$0.061^{+0.225}_{-0.300}$	$6.623^{+0.670}_{-0.670}$	$0.347^{+0.033}_{-0.045}$	-0.715 ± 0.103	0.754 ± 0.083	11.64 ± 4.42	—	—	—	
ϕ CDM	$H(z)$ + BAO	$0.0321^{+0.0060}_{-0.0060}$	$0.0847^{+0.0179}_{-0.0178}$	0.272 ± 0.028	—	$-0.076^{+0.106}_{-0.106}$	$6.557^{+0.697}_{-0.697}$	$0.347^{+0.033}_{-0.046}$	-0.713 ± 0.104	0.760 ± 0.081	11.37 ± 4.35	$0.420^{+0.029}_{-0.036}$	50.14 ± 0.26	1.153 ± 0.094	
	HzBP ^e	$0.0321^{+0.0060}_{-0.0060}$	$0.0847^{+0.0179}_{-0.0178}$	0.272 ± 0.028	—	$-0.079^{+0.106}_{-0.106}$	$6.539^{+2.24}_{-0.856}$	$0.346^{+0.032}_{-0.045}$	-0.712 ± 0.103	0.760 ± 0.082	11.36 ± 4.40	$0.420^{+0.029}_{-0.036}$	50.14 ± 0.26	1.153 ± 0.094	

^a In the four GRB-only cases Ω_bh^2 is set to 0.0245.^b w_X corresponds to flat/non-flat XCDM and α corresponds to flat/non-flat ϕ CDM.^c $\text{km s}^{-1} \text{ Mpc}^{-1}$. In the four GRB-only cases H_0 is set to 70 $\text{km s}^{-1} \text{ Mpc}^{-1}$.^d This is the 1σ limit. The 2σ limit is set by the prior and not shown here.^e $H(z)$ + BAO.^f $H(z)$ + BAO + Platinum + A101.

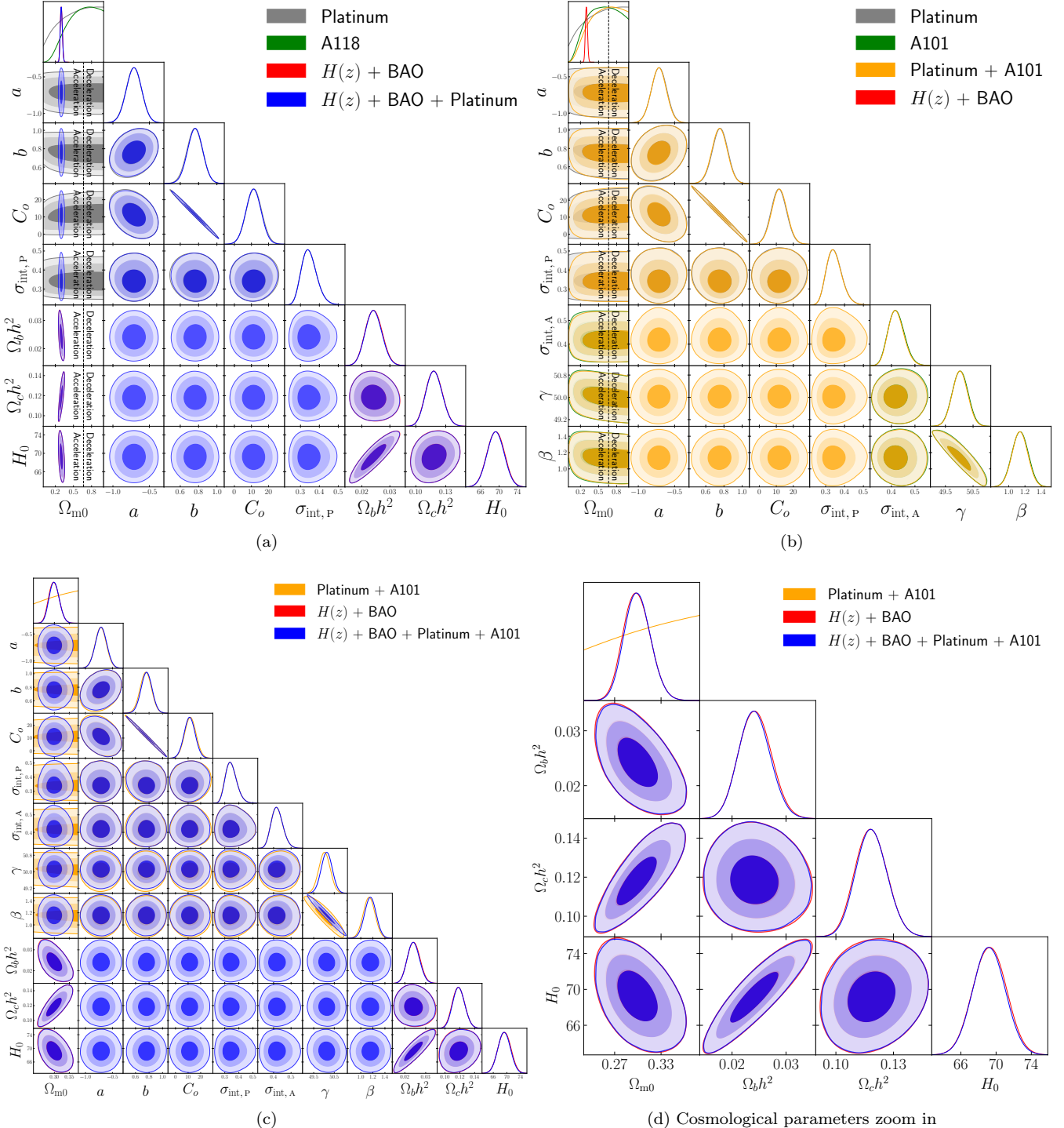


Figure 1. One-dimensional likelihood distributions and 1σ , 2σ , and 3σ two-dimensional likelihood confidence contours for flat Λ CDM from various combinations of data. The zero-acceleration black dashed lines in panels (a) and (b) divide the parameter space into regions associated with currently-accelerating (left) and currently-decelerating (right) cosmological expansion.

only 1.18σ . In both models Platinum + A101 data favor a higher 1σ lower limit of Ω_{m0} than do Platinum data or A101 data. In the non-flat Λ CDM model, the constraints on Ω_{k0} from the four GRB data sets are mutually consistent within 1σ , with all but Platinum data slightly favoring open spatial hypersurfaces. Platinum and A118 data are consistent with

flat hypersurfaces within 1σ , while A101 and Platinum + A101 data are 1.44σ and 1.17σ , respectively, away from flat. The posterior mean value of Ω_{k0} from A101 data is 1.36σ away from that from $H(z) + \text{BAO}$ data, while those from the other three GRB data sets are consistent with that from $H(z) + \text{BAO}$ data within 1σ .

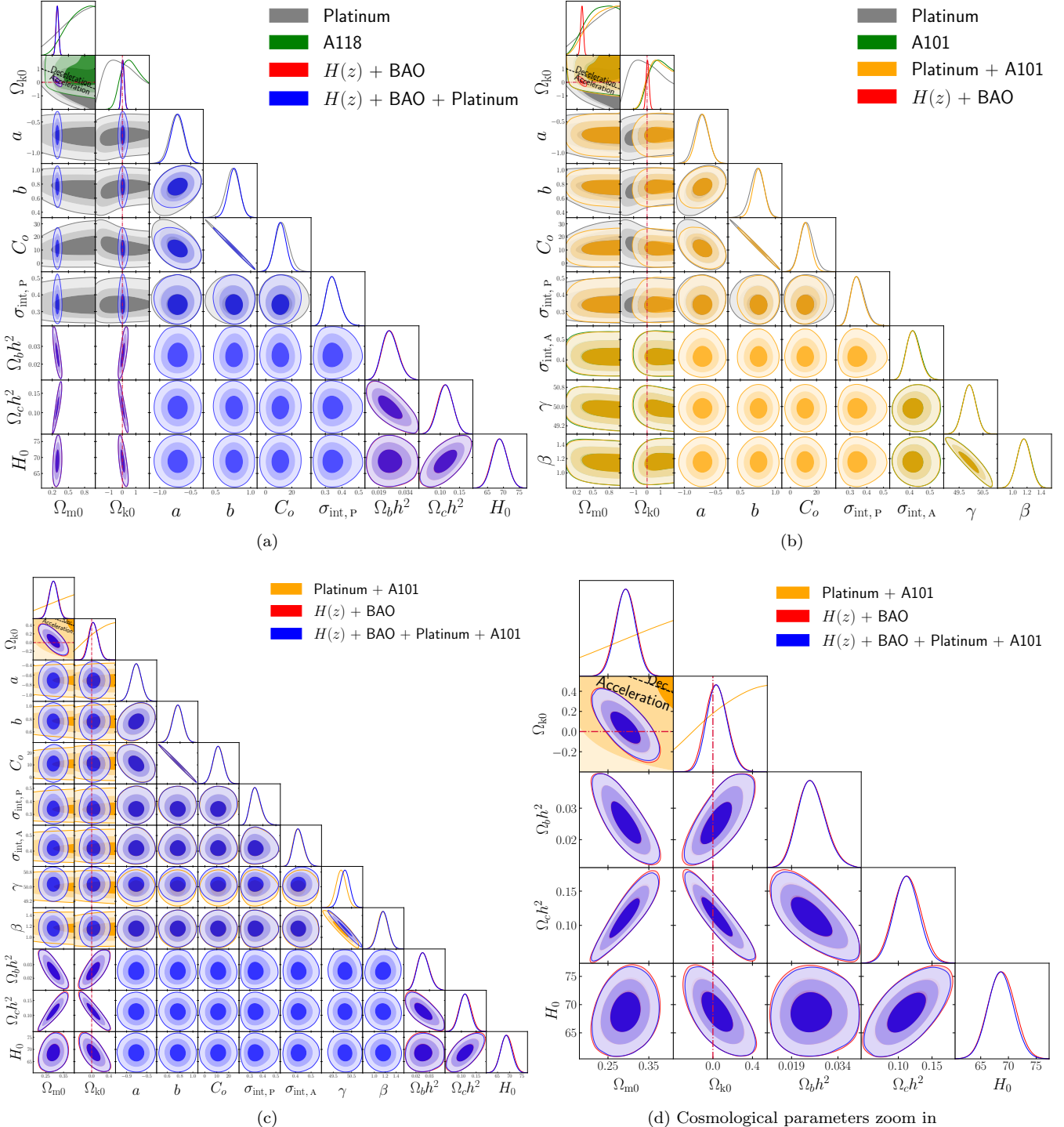


Figure 2. Same as Fig. 1 but for non-flat Λ CDM. The zero-acceleration black dashed lines divide the parameter space into regions associated with currently-accelerating (below left) and currently-decelerating (above right) cosmological expansion.

In the flat and non-flat XCDM parametrizations, the Platinum, A118, A101, and Platinum + A101 2σ constraints on Ω_{m0} are mutually consistent and also consistent with those of $H(z) + \text{BAO}$, with the 2σ lower limits in the flat (non-flat) XCDM parametrization being None (None), $> 0.181 (> 0.257)$, $> 0.148 (> 0.193)$, and $> 0.151 (> 0.207)$, respectively. In flat XCDM, the A101 constraint on Ω_{m0} is

consistent with that from $H(z) + \text{BAO}$ within 1σ . Platinum + A101 data also favor a higher 1σ lower limit of Ω_{m0} than do Platinum or A101 data in both XCDM parametrizations. The constraints on wx are weak, thus affected by the wx prior, and consistent with each other. They mildly favor phantom dark energy, but Λ is less than 1σ away, except for the flat XCDM Platinum and Platinum + A101 cases

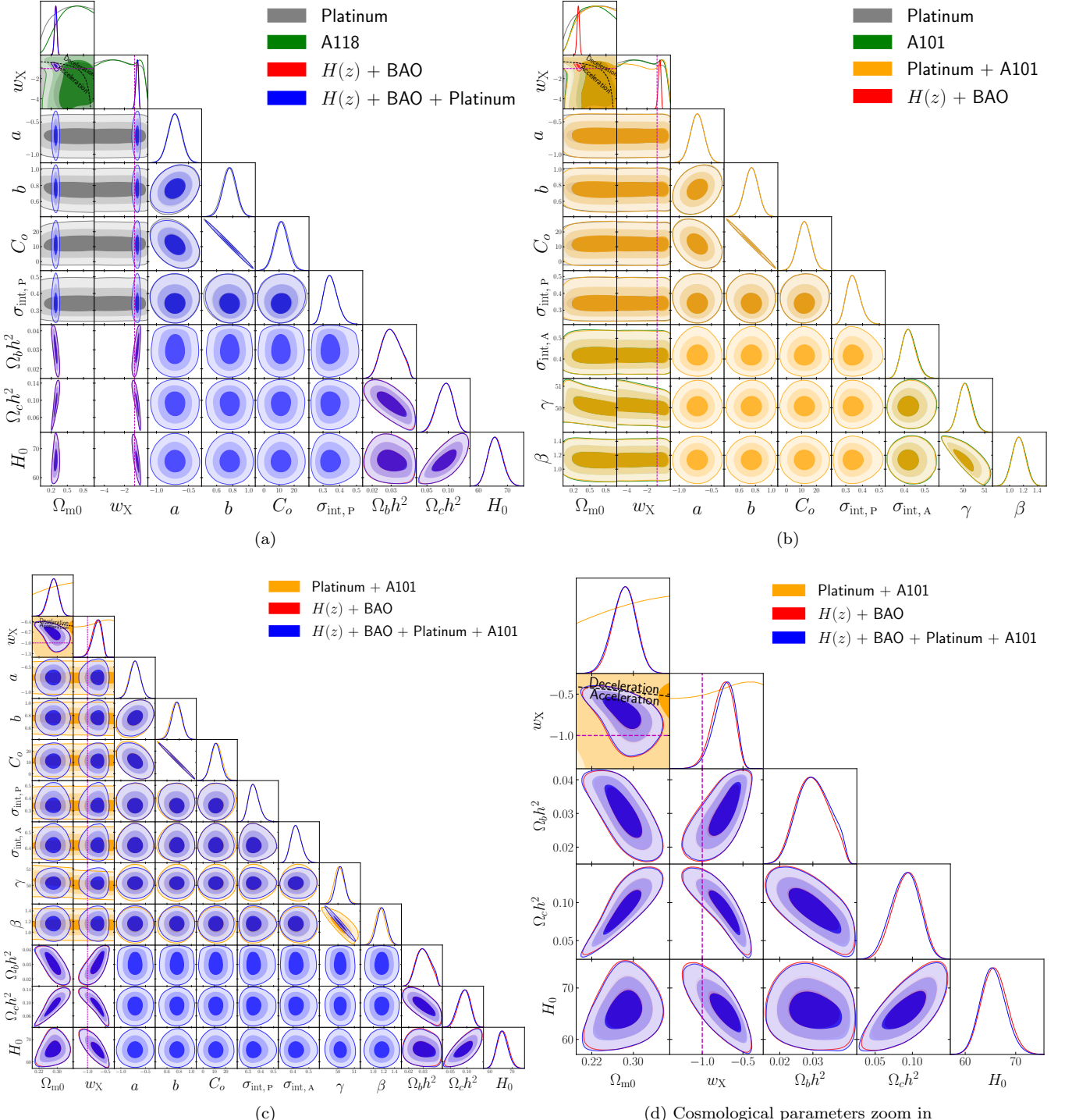


Figure 3. One-dimensional likelihood distributions and 1σ , 2σ , and 3σ two-dimensional likelihood confidence contours for flat XCDM from various combinations of data. The zero-acceleration black dashed lines divide the parameter space into regions associated with currently-accelerating (either below left or below) and currently-decelerating (either above right or above) cosmological expansion. The magenta dashed lines represent $w_X = -1$, i.e. flat Λ CDM.

(where Λ is still within 2σ), as is the case for the w_X constraints from $H(z) + \text{BAO}$ data.⁷ In non-flat XCDM, the

⁷ These are computed 2σ constraints, not necessarily twice the 1σ ones, and are not shown in the table.

constraints on Ω_{k0} from the four GRB data sets are mutually consistent within 1σ , and they slightly favor open hypersurfaces. Platinum, A118, and Platinum + A101 data are consistent with flat hypersurfaces within 1σ , while A101 data are 1.10σ away from flat. The posterior mean value of

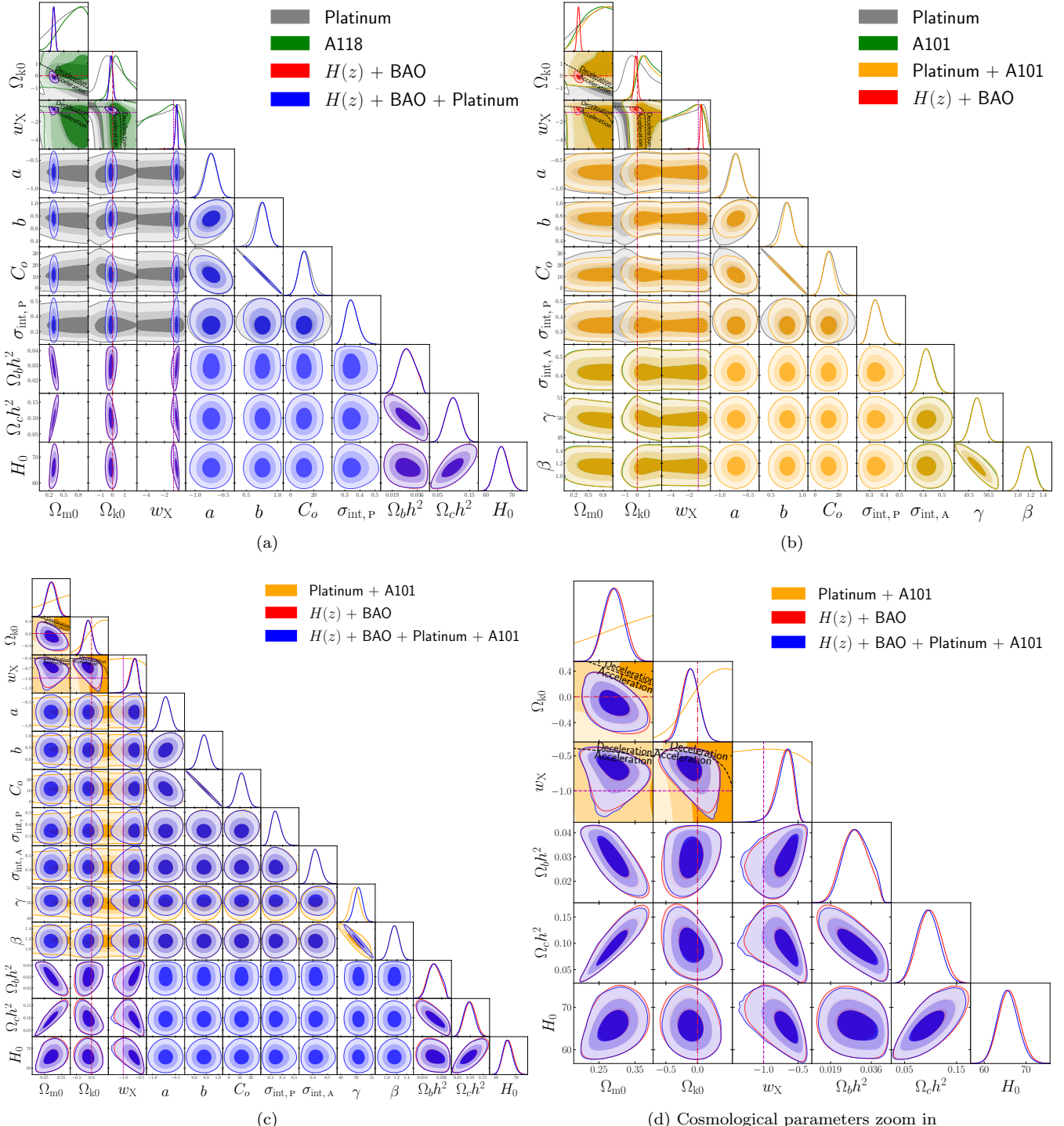


Figure 4. Same as Fig. 3 but for non-flat XCDM. The zero-acceleration black dashed lines are computed for the third cosmological parameter set to the $H(z) + \text{BAO}$ data best-fitting values listed in Table 3, and divide the parameter space into regions associated with currently-accelerating (either below left or below) and currently-decelerating (either above right or above) cosmological expansion. The crimson dash-dot lines represent flat hypersurfaces, with closed spatial hypersurfaces either below or to the left. The magenta dashed lines represent $w_X = -1$, i.e. non-flat ΛCDM .

$\Omega_{\text{k}0}$ from A101 data is 1.24σ away from that from $H(z) + \text{BAO}$ data, while those from the other three GRB data sets are consistent with that from $H(z) + \text{BAO}$ data within 1σ .

In the flat and non-flat ϕCDM models, the Platinum, A118, A101, and Platinum + A101 constraints on $\Omega_{\text{m}0}$ are

mutually consistent within 1σ and the A101 and Platinum + A101 (Platinum and A118) constraints are within 1σ (2σ) of those from $H(z) + \text{BAO}$ data. Only A118 and A101 data provide (very weak) constraints on α with Λ being more than 1σ away but within 2σ . In non-flat ϕCDM , the constraints

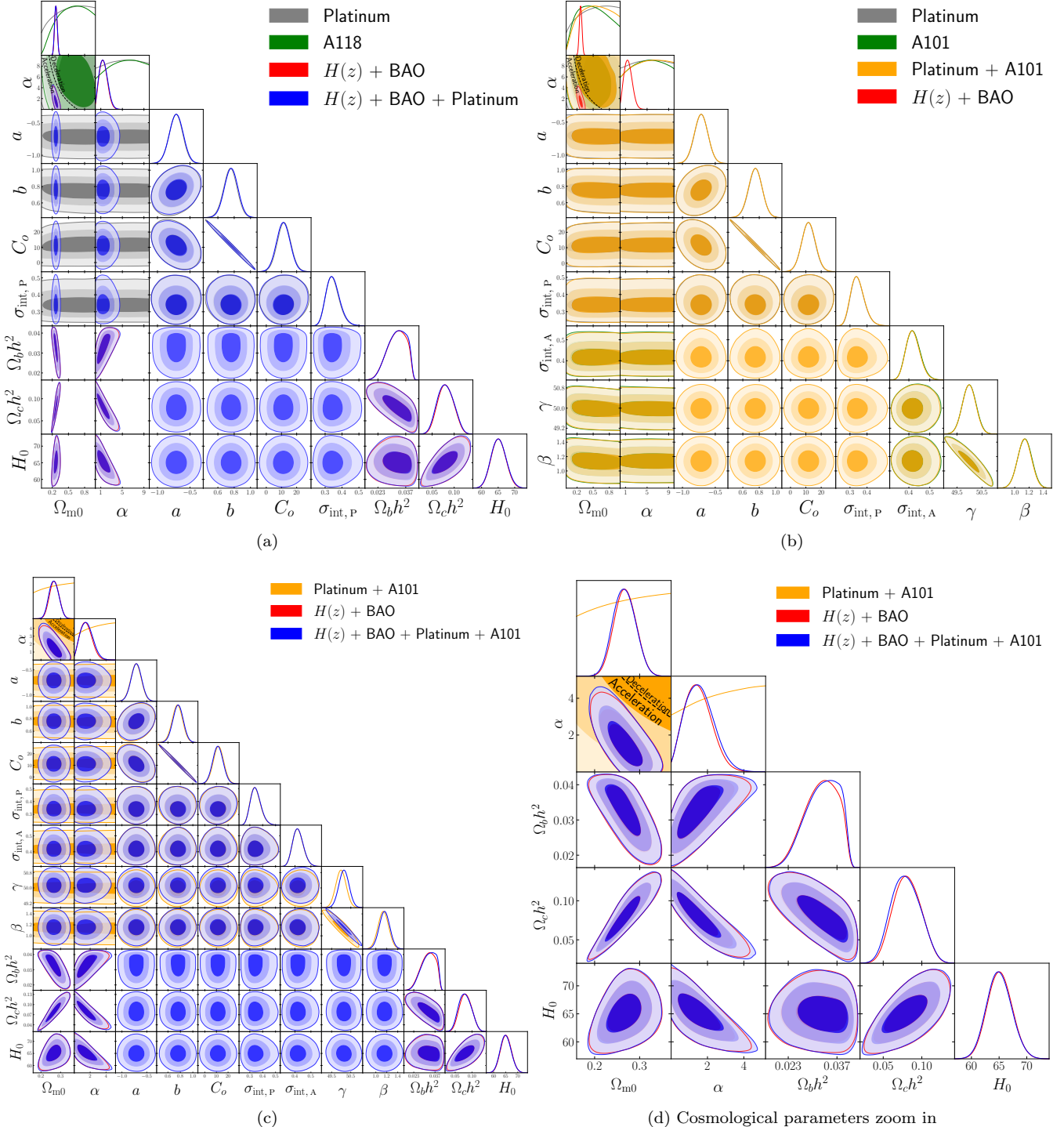


Figure 5. One-dimensional likelihood distributions and 1σ , 2σ , and 3σ two-dimensional likelihood confidence contours for flat ϕ CDM from various combinations of data. The zero-acceleration black dashed lines divide the parameter space into regions associated with currently-accelerating (below left) and currently-decelerating (above right) cosmological expansion. The $\alpha = 0$ axes correspond to flat Λ CDM.

on Ω_{k0} from the four GRB data sets are mutually consistent and consistent with that from $H(z) + \text{BAO}$ data and flat hypersurfaces are within 1σ .

From the ΔAIC and ΔBIC values listed in Table 3, in the Platinum case, non-flat Λ CDM is the most favored model, while the evidence against other models are posi-

tive, strong, and very strong (non-flat ϕ CDM). In the A118, A101, and Platinum + A101 cases, the flat Λ CDM model is the most favored model and, except for non-flat XCDM and non-flat ϕ CDM (with strong BIC evidence against them), the evidence against other models are either weak or positive. However, based on ΔDIC , in these cases, flat ϕ CDM

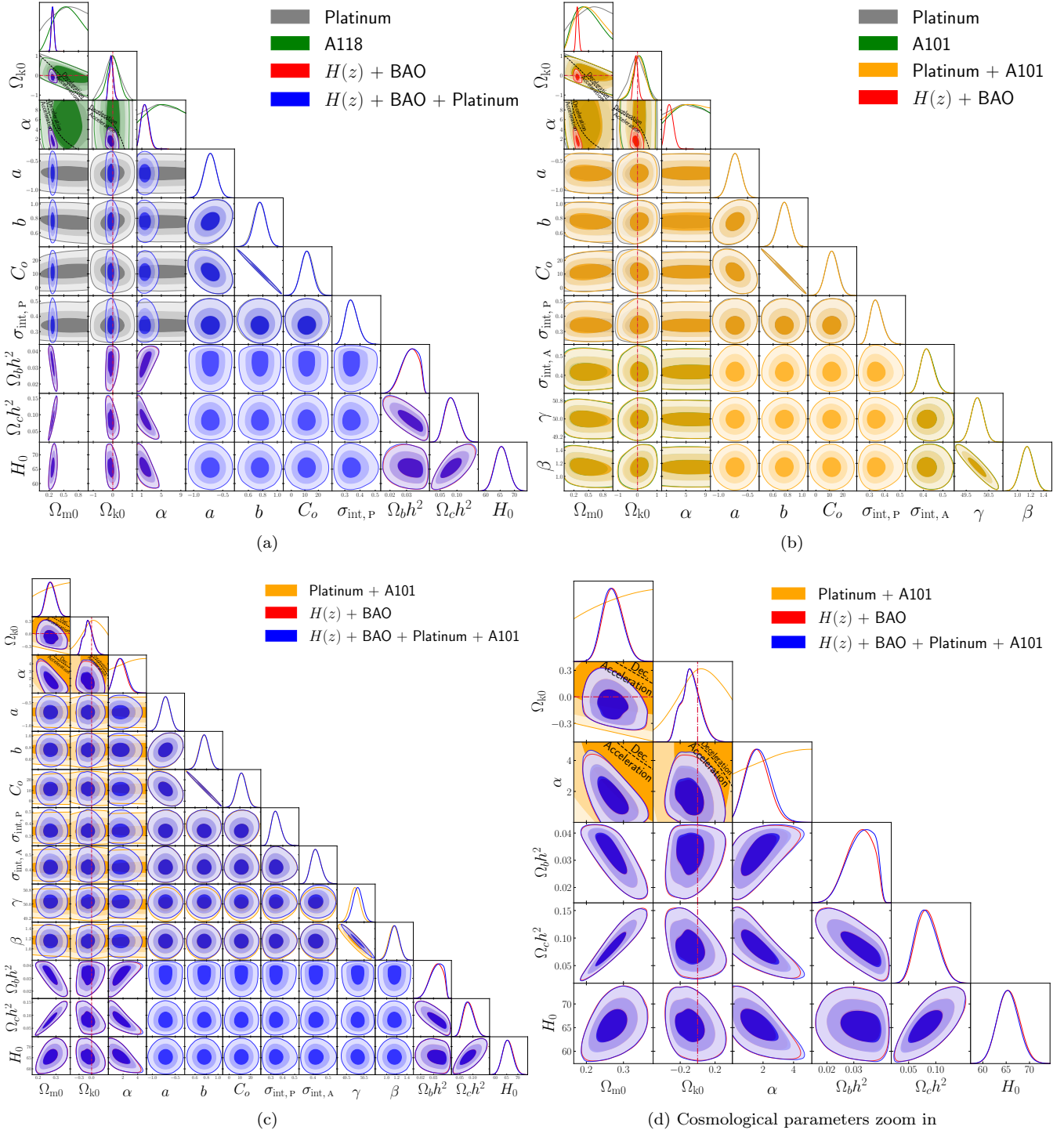


Figure 6. Same as Fig. 5 but for non-flat ϕ CDM. The zero-acceleration black dashed lines are computed for the third cosmological parameter set to the $H(z)$ + BAO data best-fitting values listed in Table 3, and divide the parameter space into regions associated with currently-accelerating (below left) and currently-decelerating (above right) cosmological expansion. The crimson dash-dot lines represent flat hypersurfaces, with closed spatial hypersurfaces either below or to the left. The $\alpha = 0$ axes correspond to non-flat Λ CDM.

is the most favored model; in the A118, A101, and Platinum + A101 cases, the evidence against other models are weak; whereas in the Platinum case, the evidence against other models are either weak or strong (non-flat Λ CDM and non-flat XCDM).

5.2 Constraints from $H(z)$ + BAO data in combination with Platinum (HzBP) and Platinum + A101 (HzBPA101) data

Since the $H(z)$ + BAO, Platinum, and Platinum + A101 cosmological constraints are mutually consistent, we jointly

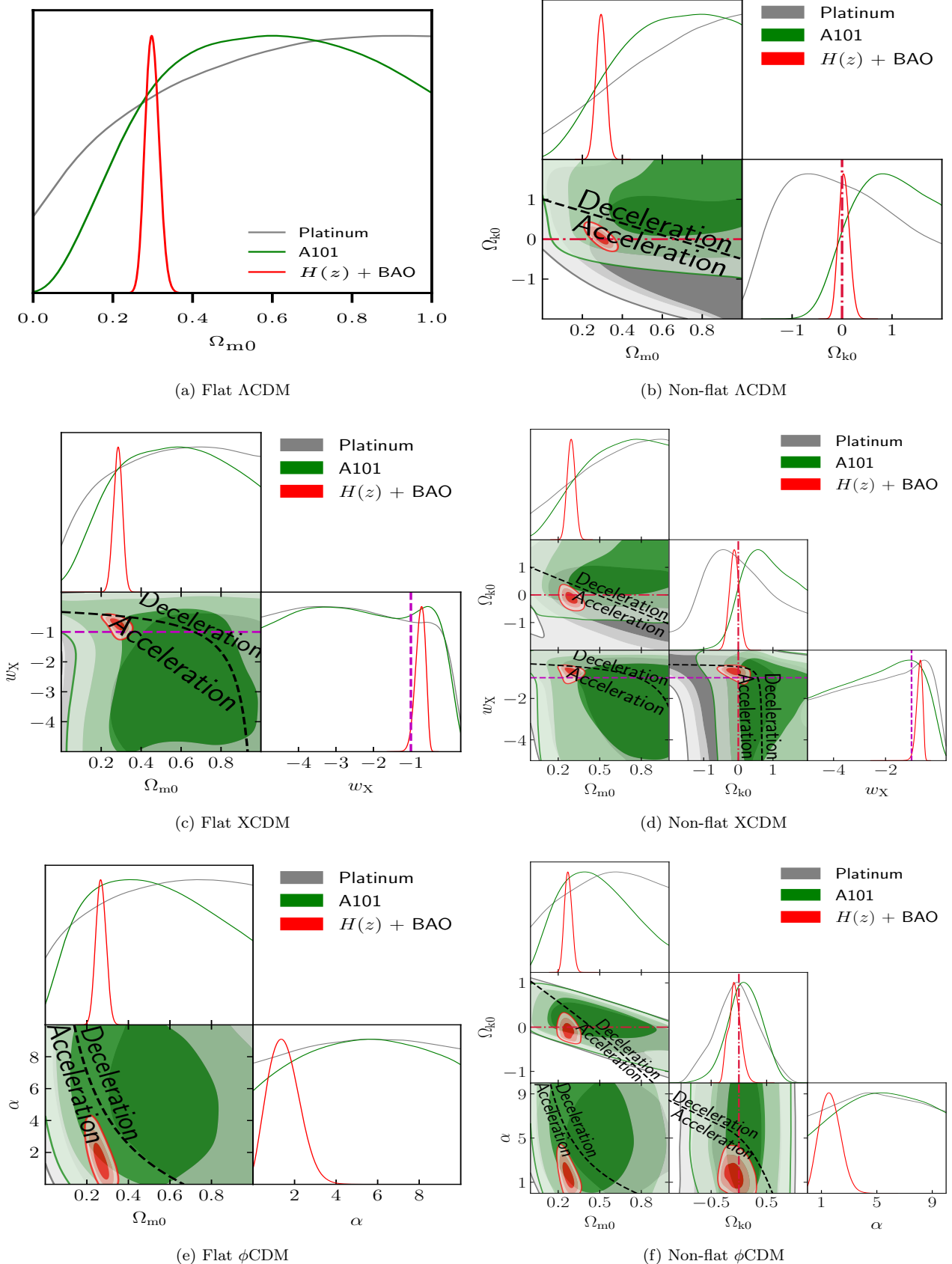


Figure 7. One-dimensional likelihood distributions and 1σ , 2σ , and 3σ two-dimensional likelihood confidence contours for some cosmological parameters of the six cosmological models from Platinum data (gray), A101 data (green), and $H(z)$ + BAO data (red), which more clearly show the cosmological parameter overlaps between Platinum/A101 data and $H(z)$ + BAO data.

analyze combinations of these data to determine more restrictive constraints on cosmological and GRB correlation parameters. We find that the new constraints on GRB correlation parameters are more restrictive but change less than 1σ compared to those from the GRB-only analyses. The correlation parameter constraints remain cosmological-model-independent, indicating again that these GRBs are standardizable. In what follows we discuss how the $H(z) + \text{BAO}$ data cosmological parameter constraints are altered when these GRB data are jointly analyzed with $H(z) + \text{BAO}$ data.

Compared to the $H(z) + \text{BAO}$ constraints, the HzBP constraints on Ω_{m0} are almost unchanged in all models, but there are small changes in other cosmological parameter constraints. The constraints on H_0 are slightly tightened, with posterior means being $0.01 - 0.03\sigma$ smaller or larger from model to model; the constraints on w_X are slightly shifted away from Λ , with posterior means being $\sim 0.04\sigma$ larger; the constraints on α are slightly shifted away from Λ , with posterior means being 0.02σ (0.05σ) larger in flat (non-flat) ϕCDM ; and the constraints on Ω_{k0} are slightly shifted away from flat, with posterior means being 0.06σ (0.10σ) smaller in non-flat XCDM (ϕCDM).

Compared to $H(z) + \text{BAO}$, the HzBPA101 data provide mildly different constraints on Ω_{m0} in all models, but the effects on other cosmological parameter constraints are more noticeable. The constraints on H_0 are slightly tightened, with posterior means being $0.03 - 0.10\sigma$ smaller from model to model; the constraints on w_X are slightly shifted away from Λ , with posterior means being 0.11σ (0.08σ) larger in flat (non-flat) XCDM; the constraints on α are slightly shifted away from Λ , with posterior means being 0.07σ (0.08σ) larger in flat (non-flat) ϕCDM ; and the constraints on Ω_{k0} are slightly shifted towards (away) from flat, with posterior means being 0.05σ (0.02σ) larger (smaller) in non-flat XCDM (ϕCDM), respectively.

From the ΔAIC , ΔBIC , and ΔDIC values listed in Table 3, in both the HzBP and the HzBPA101 cases, following the patterns of the $H(z) + \text{BAO}$ case, flat ϕCDM is the most favored model but the evidence against other models are only either weak or positive. As expected, the better-established $H(z) + \text{BAO}$ data play the dominant role in these combined analyses and therefore currently accelerating cosmological expansion is favored.

6 CONCLUSION

We have analyzed the 50 Platinum GRBs, that obey the three-parameter fundamental plane (or Dainotti) relation, using six different cosmological models. By simultaneously constraining cosmological model and GRB correlation parameters our approach circumvents the circularity problem. We find that the Platinum GRB correlation parameters are cosmological-model-independent so the Platinum sample is standardizable through the three-parameter Dainotti correlation and can be used to constrain cosmological parameters. Since the cosmological constraints from Platinum data are consistent with those from $H(z) + \text{BAO}$ data, we have combined Platinum and $H(z) + \text{BAO}$ data to perform a joint (HzBP) analysis and find mild changes of the cosmological parameter constraints relative to those from $H(z) + \text{BAO}$

data, with the central values in the two cases agreeing to two significant figures.

We have also reanalyzed the A118 GRBs that obey the Amati ($E_p - E_{iso}$) correlation (Khadka et al. 2021c; Cao et al. 2022b), because of different, improved modeling of neutrino physics here, and, by excluding the 17 overlapping (with Platinum) GRBs from the larger A118 data set to form the truncated A101 data set, we have also performed a joint analysis of Platinum and A101 data. The twice as large A101 data set plays a dominant role in the joint Platinum + A101 analysis, and the cosmological constraints from Platinum + A101 data are closer to those from A101 data. The results show that the Platinum + A101 GRBs are also standardizable and their cosmological constraints are also more consistent (than the A118 ones) with those from $H(z) + \text{BAO}$ data. The joint analyses of $H(z) + \text{BAO}$ and Platinum + A101 (HzBPA101) data show that Platinum + A101 data do have more impact on the joint constraints than do Platinum data, however, $H(z) + \text{BAO}$ data still play the dominant role.

Current compilations of GRBs provide some improvements on the cosmological constraints determined using $H(z) + \text{BAO}$ data. Importantly, GRBs are the only currently reliable probes of the $z \sim 3 - 8$ part of cosmological redshift space and so are well worth improving upon. With the upcoming SVOM mission (Cordier 2019) in 2023, and possibly Theseus (Amati et al. 2021) in 2037 if approved in the new ESA call, there soon will be larger GRB data sets over a wider range of redshifts that will allow for improved GRB cosmological constraints.

ACKNOWLEDGEMENTS

This research was supported in part by DOE grant DE-SC0011840. The computations for this project were performed on the Beocat Research Cluster at Kansas State University, which is funded in part by NSF grants CNS-1006860, EPS-1006860, EPS-0919443, ACI-1440548, CHE-1726332, and NIH P20GM113109.

DATA AVAILABILITY

The data underlying this article are listed in Table A1.

REFERENCES

- Amati L., Guidorzi C., Frontera F., Della Valle M., Finelli F., Landi R., Montanari E., 2008, *MNRAS*, **391**, 577
- Amati L., D'Agostino R., Luongo O., Muccino M., Tantalo M., 2019, *MNRAS*, **486**, L46
- Amati L., et al., 2021, *Experimental Astronomy*, **52**, 183
- Arjona R., Nesseris S., 2021, *Phys. Rev. D*, **103**, 103539
- Blas D., Lesgourgues J., Tram T., 2011, *J. Cosmology Astropart. Phys.*, **2011**, 034
- Brinckmann T., Lesgourgues J., 2019, *Physics of the Dark Universe*, **24**, 100260
- Cao S., Biesiada M., Jackson J., Zheng X., Zhao Y., Zhu Z.-H., 2017, *J. Cosmology Astropart. Phys.*, **2**, 012
- Cao S., Ryan J., Ratra B., 2020, *MNRAS*, **497**, 3191
- Cao S., Ryan J., Khadka N., Ratra B., 2021a, *MNRAS*, **501**, 1520
- Cao S., Ryan J., Ratra B., 2021b, *MNRAS*, **504**, 300

- Cao S., Ryan J., Ratra B., 2022a, *MNRAS*, **509**, 4745
 Cao S., Khadka N., Ratra B., 2022b, *MNRAS*, **510**, 2928
 Cardone V. F., Capozziello S., Dainotti M. G., 2009, *MNRAS*, **400**, 775
 Cardone V. F., Dainotti M. G., Capozziello S., Willingale R., 2010, *MNRAS*, **408**, 1181
 Chávez R., Terlevich R., Terlevich E., Bresolin F., Melnick J., Plionis M., Basilakos S., 2014, *MNRAS*, **442**, 3565
 Chen Y., Ratra B., Biesiada M., Li S., Zhu Z.-H., 2016, *ApJ*, **829**, 61
 Chen Y., Kumar S., Ratra B., 2017, *ApJ*, **835**, 86
 Cordier B., 2019, *Mem. Soc. Ast. It.*, **90**, 242
 Cucchiara A., et al., 2011, *ApJ*, **736**, 7
 Czerny B., et al., 2021, *Acta Physica Polonica A*, **139**, 389
 D'Agostini G., 2005, preprint, ([arXiv:physics/0511182](https://arxiv.org/abs/physics/0511182))
 DES Collaboration 2019, *Phys. Rev. D*, **99**, 123505
 Dai Y., Zheng X.-G., Li Z.-X., Gao H., Zhu Z.-H., 2021, *A&A*, **651**, L8
 Dainotti M. G., Cardone V. F., Capozziello S., 2008, *MNRAS*, **391**, L79
 Dainotti M. G., Willingale R., Capozziello S., Fabrizio Cardone V., Ostrowski M., 2010, *ApJ*, **722**, L215
 Dainotti M. G., Fabrizio Cardone V., Capozziello S., Ostrowski M., Willingale R., 2011, *ApJ*, **730**, 135
 Dainotti M. G., Cardone V. F., Piedipalumbo E., Capozziello S., 2013a, *MNRAS*, **436**, 82
 Dainotti M. G., Petrosian V., Singal J., Ostrowski M., 2013b, *ApJ*, **774**, 157
 Dainotti M., Petrosian V., Willingale R., O'Brien P., Ostrowski M., Nagataki S., 2015, *MNRAS*, **451**, 3898
 Dainotti M. G., Postnikov S., Hernandez X., Ostrowski M., 2016, *ApJ*, **825**, L20
 Dainotti M. G., Nagataki S., Maeda K., Postnikov S., Pian E., 2017, *A&A*, **600**, A98
 Dainotti M. G., Lenart A. L., Sarracino G., Nagataki S., Capozziello S., Fraija N., 2020, *ApJ*, **904**, 97
 Dainotti M. G., Lenart A. L., Fraija N., Nagataki S., Warren D. C., De Simone B., Srinivasaragavan G., Mata A., 2021a, *PASJ*, **73**, 970
 Dainotti M. G., De Simone B., Schiavone T., Montani G., Rinaldi E., Lambiase G., 2021b, *ApJ*, **912**, 150
 Dainotti M. G., De Simone B. D., Schiavone T., Montani G., Rinaldi E., Lambiase G., Bogdan M., Ugale S., 2022, *Galaxies*, **10**, 24
 de Cruz Perez J., Sola Peracaula J., Gomez-Valent A., Moreno-Pulido C., 2021, preprint, ([arXiv:2110.07569](https://arxiv.org/abs/2110.07569))
 Demianski M., Piedipalumbo E., Sawant D., Amati L., 2021, *MNRAS*, **506**, 903
 Dhawan S., Alsing J., Vagnozzi S., 2021, *MNRAS*, **506**, L1
 Di Valentino E., et al., 2021a, *Classical and Quantum Gravity*, **38**, 153001
 Di Valentino E., Melchiorri A., Silk J., 2021b, *ApJ*, **908**, L9
 eBOSS Collaboration 2021, *Phys. Rev. D*, **103**, 083533
 Efstathiou G., Gratton S., 2020, *MNRAS*, **496**, L91
 Fana Dirirsa F., et al., 2019, *ApJ*, **887**, 13
 Farooq O., Ranjeet Madiyar F., Crandall S., Ratra B., 2017, *ApJ*, **835**, 26
 Geng C.-Q., Hsu Y.-T., Lu J.-R., 2022, *ApJ*, **926**, 74
 González-Morán A. L., et al., 2019, *MNRAS*, **487**, 4669
 González-Morán A. L., et al., 2021, *MNRAS*, **505**, 1441
 Handley W., 2019, *Phys. Rev. D*, **100**, 123517
 Hu J. P., Wang F. Y., Dai Z. G., 2021, *MNRAS*, **507**, 730
 Jesus J. F., Valentim R., Escobal A. A., Pereira S. H., Benndorf D., 2021, preprint, ([arXiv:2112.09722](https://arxiv.org/abs/2112.09722))
 Johnson J. P., Sangwan A., Shankaranarayanan S., 2022, *J. Cosmology Astropart. Phys.*, **2022**, 024
 Khadka N., Ratra B., 2020a, *MNRAS*, **492**, 4456
 Khadka N., Ratra B., 2020b, *MNRAS*, **497**, 263
 Khadka N., Ratra B., 2020c, *MNRAS*, **499**, 391
 Khadka N., Ratra B., 2021, *MNRAS*, **502**, 6140
 Khadka N., Ratra B., 2022, *MNRAS*, **510**, 2753
 Khadka N., Martínez-Aldama M. L., Zajaček M., Czerny B., Ratra B., 2021a, preprint, ([arXiv:2112.00052](https://arxiv.org/abs/2112.00052))
 Khadka N., Yu Z., Zajaček M., Martínez-Aldama M. L., Czerny B., Ratra B., 2021b, *MNRAS*, **508**, 4722
 Khadka N., Luongo O., Muccino M., Ratra B., 2021c, *J. Cosmology Astropart. Phys.*, **2021**, 042
 KiDS Collaboration 2021, *A&A*, **649**, A88
 Kunz M., Trotta R., Parkinson D. R., 2006, *Phys. Rev. D*, **74**, 023503
 Lamb D. Q., Reichart D. E., 2000, *ApJ*, **536**, 1
 Lewis A., 2019, preprint, ([arXiv:1910.13970](https://arxiv.org/abs/1910.13970))
 Li E.-K., Du M., Xu L., 2020, *MNRAS*, **491**, 4960
 Li X., Keeley R. E., Shafieloo A., Zheng X., Cao S., Biesiada M., Zhu Z.-H., 2021, *MNRAS*, **507**, 919
 Lian Y., Cao S., Biesiada M., Chen Y., Zhang Y., Guo W., 2021, *MNRAS*, **505**, 2111
 Luongo O., Muccino M., 2021, *Galaxies*, **9**
 Luongo O., Muccino M., Colgáin E. Ó., Sheikh-Jabbari M. M., Yin L., 2021, preprint, ([arXiv:2108.13228](https://arxiv.org/abs/2108.13228))
 Lusso E., et al., 2020, *A&A*, **642**, A150
 Mania D., Ratra B., 2012, *Physics Letters B*, **715**, 9
 Mehrabi A., et al., 2022, *MNRAS*, **509**, 224
 Ooba J., Ratra B., Sugiyama N., 2018a, *ApJ*, **864**, 80
 Ooba J., Ratra B., Sugiyama N., 2018b, *ApJ*, **866**, 68
 Ooba J., Ratra B., Sugiyama N., 2018c, *ApJ*, **869**, 34
 Ooba J., Ratra B., Sugiyama N., 2019, *Ap&SS*, **364**, 176
 Park C.-G., Ratra B., 2018, *ApJ*, **868**, 83
 Park C.-G., Ratra B., 2019a, *Ap&SS*, **364**, 82
 Park C.-G., Ratra B., 2019b, *Ap&SS*, **364**, 134
 Park C.-G., Ratra B., 2019c, *ApJ*, **882**, 158
 Park C.-G., Ratra B., 2020, *Phys. Rev. D*, **101**, 083508
 Pavlov A., Westmoreland S., Saaidi K., Ratra B., 2013, *Phys. Rev. D*, **88**, 123513
 Peebles P. J. E., 1984, *ApJ*, **284**, 439
 Peebles P. J. E., Ratra B., 1988, *ApJ*, **325**, L17
 Perivolaropoulos L., Skara F., 2021, preprint, ([arXiv:2105.05208](https://arxiv.org/abs/2105.05208))
 Planck Collaboration 2020, *A&A*, **641**, A6
 Postnikov S., Dainotti M. G., Hernandez X., Capozziello S., 2014, *ApJ*, **783**, 126
 Rana A., Jain D., Mahajan S., Mukherjee A., 2017, *J. Cosmology Astropart. Phys.*, **2017**, 028
 Ratra B., Peebles P. J. E., 1988, *Phys. Rev. D*, **37**, 3406
 Renzi F., Hogg N. B., Giarè W., 2021, preprint, ([arXiv:2112.05701](https://arxiv.org/abs/2112.05701))
 Rezaei M., Solà Peracaula J., Malekjani M., 2021, *MNRAS*, **509**, 2593
 Risaliti G., Lusso E., 2015, *ApJ*, **815**, 33
 Risaliti G., Lusso E., 2019, *Nature Astronomy*, **3**, 272
 Ryan J., Doshi S., Ratra B., 2018, *MNRAS*, **480**, 759
 Ryan J., Chen Y., Ratra B., 2019, *MNRAS*, **488**, 3844
 Samushia L., Ratra B., 2010, *ApJ*, **714**, 1347
 Sangwan A., Tripathi A., Jassal H. K., 2018, preprint, ([arXiv:1804.09350](https://arxiv.org/abs/1804.09350))
 Scolnic D. M., et al., 2018, *ApJ*, **859**, 101
 Singh A., Sangwan A., Jassal H. K., 2019, *J. Cosmology Astropart. Phys.*, **2019**, 047
 Sinha S., Banerjee N., 2021, *J. Cosmology Astropart. Phys.*, **2021**, 060
 Solà Peracaula J., Gómez-Valent A., de Cruz Pérez J., 2019, *Physics of the Dark Universe*, **25**, 100311
 Ureña-López L. A., Roy N., 2020, *Phys. Rev. D*, **102**, 063510
 Vagnozzi S., Di Valentino E., Gariazzo S., Melchiorri A., Mena O., Silk J., 2021a, *Physics of the Dark Universe*, **33**, 100851
 Vagnozzi S., Loeb A., Moresco M., 2021b, *ApJ*, **908**, 84

- Wang F. Y., Dai Z. G., Liang E. W., 2015, *New Astron. Rev.*, **67**, 1
- Wang J. S., Wang F. Y., Cheng K. S., Dai Z. G., 2016, *A&A*, **585**, A68
- Wang F. Y., Hu J. P., Zhang G. Q., Dai Z. G., 2022, *ApJ*, **924**, 97
- Wei J.-J., 2018, *ApJ*, **868**, 29
- Willingale R., et al., 2007, *ApJ*, **662**, 1093
- Willingale R., Genet F., Granot J., O'Brien P. T., 2010, *MNRAS*, **403**, 1296
- Xu T., Chen Y., Xu L., Cao S., 2021, preprint, ([arXiv:2109.02453](https://arxiv.org/abs/2109.02453))
- Yang T., Banerjee A., Ó Colgáin E., 2020, *Phys. Rev. D*, **102**, 123532
- Yu H., Ratra B., Wang F.-Y., 2018, *ApJ*, **856**, 3
- Yu Z., et al., 2021, *MNRAS*, **507**, 3771
- Zajaček M., et al., 2021, *ApJ*, **912**, 10
- Zhai Z., Blanton M., Slosar A., Tinker J., 2017, *ApJ*, **850**, 183
- Zhang C., Zhang H., Yuan S., Liu S., Zhang T.-J., Sun Y.-C., 2014, *Research in Astronomy and Astrophysics*, **14**, 1221
- Zhao D., Xia J.-Q., 2021, *European Physical Journal C*, **81**, 694
- Zheng X., Cao S., Biesiada M., Li X., Liu T., Liu Y., 2021, *Science China Physics, Mechanics, and Astronomy*, **64**, 259511

APPENDIX A: PLATINUM GRB DATA

This paper has been typeset from a TeX/LaTeX file prepared by the author.

Table A1. 50 Platinum GRB samples.

GRB	z	$\log T_X^* \text{ (s)}$	$\log F_X \text{ (erg cm}^{-2} \text{ s}^{-1}\text{)}$	β'	$F_{\text{peak}} \text{ (10}^{-8} \text{ erg cm}^{-2} \text{ s}^{-1}\text{)}$
060418	1.49	$3.11887^{+0.05725}_{-0.05724}$	-9.79296 ± 0.04904	1.98	49.9 ± 1.63
060605	3.8	$4.04162^{+0.03738}_{-0.03737}$	$-11.2609^{+0.0531}_{-0.0532}$	1.835	4.73 ± 0.693
060708	1.92	$3.50569^{+0.06273}_{-0.06272}$	$-10.8688^{+0.0611}_{-0.0612}$	2.485	6.89 ± 0.796
060714	2.71	$3.73449^{+0.04676}_{-0.04677}$	-10.8586 ± 0.0352	1.87	9.13 ± 0.549
060814	0.84	$4.22387^{+0.03485}_{-0.03486}$	-10.9108 ± 0.0353	1.97	60.6 ± 1.48
060906	3.685	$4.33479^{+0.07214}_{-0.07215}$	$-11.8833^{+0.0885}_{-0.0884}$	2.06	12.2 ± 1.18
061121	1.314	3.78753 ± 0.01703	$-10.0299^{+0.0126}_{-0.0127}$	1.9485	196 ± 2.43
061222A	2.088	$3.92091^{+0.02444}_{-0.02443}$	-9.95369 ± 0.02311	1.86	73.3 ± 1.51
070110	2.352	$4.26825^{+0.05399}_{-0.05400}$	$-11.0488^{+0.0547}_{-0.0548}$	2.186	4.73 ± 0.648
070306	1.4959	4.86926 ± 0.02824	-11.2737 ± 0.0335	1.831	20.1 ± 0.899
070508	0.82	3.02525 ± 0.01189	$-9.16118^{+0.01080}_{-0.01079}$	1.764	224 ± 3.07
070521	0.553	3.55243 ± 0.04844	$-10.01250^{+0.04902}_{-0.04900}$	1.98	8.71 ± 1.2
070529	2.4996	$3.09323^{+0.06805}_{-0.06804}$	-10.2468 ± 0.0552	1.76	11.1 ± 1.84
080310	2.4266	$4.326080559^{+0.037986760}_{-0.037986759}$	$-11.39909559 \pm 0.04247343$	1.878	7.52 ± 0.893
080430	0.767	$4.217629106^{+0.038388523}_{-0.038388522}$	$-11.17223461^{+0.02818096}_{-0.02818097}$	4.18	18.2 ± 0.808
080721	2.6	$2.878762860^{+0.007554815}_{-0.007554816}$	$-8.713485538^{+0.007019298}_{-0.007019299}$	1.735	193 ± 10.3
081008	1.967	$3.855508334 \pm 0.056285684$	$-10.79325557 \pm 0.06052989$	1.84	10.5 ± 0.813
081221	2.26	$2.931957486 \pm 0.031176651$	$-9.354590372 \pm 0.024985500$	1.991	147 ± 2.46
090418A	1.608	$3.528136567^{+0.030759021}_{-0.030759020}$	$-10.04734554^{+0.02865941}_{-0.02865940}$	1.98	15.8 ± 1.66
091018	0.971	$2.896555345^{+0.034497877}_{-0.034497878}$	$-9.626765539^{+0.024288604}_{-0.024288603}$	1.91	59.1 ± 1.22
091020	1.71	$2.952650108 \pm 0.045271255$	$-9.712875280 \pm 0.034480687$	1.895	36.4 ± 1.71
091029	2.752	$4.303689975^{+0.034224003}_{-0.034224002}$	$-11.34682089 \pm 0.02563352$	2.064	10.9 ± 0.786
100219A	4.7	$4.721899099 \pm 0.103773463$	$-12.13530676^{+0.32639562}_{-0.32639563}$	1.46	3.15 ± 0.721
110213A	1.46	$3.84089^{+0.02576}_{-0.02127}$	$-9.89698^{+0.03865}_{-0.03311}$	2.1905	7.15 ± 1.88
110818A	3.36	$3.846274153 \pm 0.059648416$	$-11.28292779 \pm 0.05514905$	1.83	14.1 ± 1.5
111008A	5	$3.989933926 \pm 0.035676696$	$-10.66765993^{+0.02851108}_{-0.02851109}$	1.829	54.1 ± 3.91
120118B	2.943	$3.68307^{+0.15437}_{-0.10916}$	$-10.9560^{+0.1224}_{-0.1120}$	2.01	13.8 ± 1.32
120404A	2.88	$3.79948^{+0.09188}_{-0.04469}$	$-11.0269^{+0.0927}_{-0.1414}$	1.69	7.62 ± 0.109
120811C	2.67	$3.159095907^{+0.084200302}_{-0.084200301}$	$-10.14322956 \pm 0.05294686$	1.65	26 ± 1.1
120922A	3.1	$3.59799^{+0.21328}_{-0.05347}$	$-10.5957^{+0.1158}_{-0.2115}$	2.17	10.6 ± 0.757
121128A	2.2	$3.233929220^{+0.029795567}_{-0.029795568}$	$-9.618411717^{+0.028690024}_{-0.028690023}$	1.9455	104 ± 2.1
131030A	1.29	$2.84594^{+0.02758}_{-0.02757}$	$-9.29414^{+0.02517}_{-0.02518}$	1.693	265 ± 4.61
131105A	1.686	$3.94880^{+0.04788}_{-0.04789}$	$-10.9111^{+0.0333}_{-0.0334}$	1.94	26.8 ± 0.204
140206A	2.7	$3.59073^{+0.02132}_{-0.02133}$	$-9.72980^{+0.01300}_{-0.01299}$	1.672	169 ± 2.62
140419A	3.956	3.68383 ± 0.02442	$-10.00560^{+0.02397}_{-0.02400}$	1.678	41.8 ± 1.28
140506A	0.889	3.30686 ± 0.06882	-9.90438 ± 0.05516	1.9	86.7 ± 4.56
140509A	2.4	$3.58709^{+0.11327}_{-0.06416}$	$-11.0977^{+0.0897}_{-0.0782}$	1.86	11.8 ± 1.77
140629A	2.3	2.85608 ± 0.06161	$-9.84891^{+0.04278}_{-0.04279}$	1.815	35 ± 1.87
150314A	1.758	$2.49217^{+0.01586}_{-0.01585}$	$-8.60990^{+0.01503}_{-0.01502}$	1.73	381 ± 6.06
150403A	2.06	$3.19694^{+0.06698}_{-0.06697}$	$-8.82118^{+0.00510}_{-0.00511}$	1.679	171 ± 3.81
150910A	1.36	3.85419 ± 0.02868	$-9.97065^{+1.37578}_{-0.03215}$	1.6645	8.28 ± 2.18
151027A	0.81	3.99907 ± 0.041731	-9.93519 ± 0.02221	1.9235	58.2 ± 2.88
160121A	1.96	$3.82440^{+0.12038}_{-0.12039}$	-11.1726 ± 0.0694	2.02	7.79 ± 0.823
160227A	2.38	4.47751 ± 0.03885	$-10.9957^{+0.0305}_{-0.0306}$	1.679	4.88 ± 0.688
160327A	4.99	3.76407 ± 0.06033	-11.2238 ± 0.0673	1.78	12.5 ± 0.877
170202A	3.645	$3.77629^{+0.06866}_{-0.06865}$	$-10.6535^{+0.0449}_{-0.0448}$	2.04	39.2 ± 1.79
170705A	2.01	3.63746 ± 0.06603	$-10.1867^{+0.0406}_{-0.0405}$	1.66	113 ± 2.41
180329B	1.998	4.02296 ± 0.04314	$-11.1493^{+0.0482}_{-0.0483}$	1.77	9.09 ± 2.02
190106A	1.86	$4.19124^{+0.03109}_{-0.03110}$	$-10.4325^{+0.0286}_{-0.0286}$	2.9365	33.6 ± 1.3
190114A	3.37	$3.74534^{+0.04221}_{-0.04222}$	$-10.7527^{+0.0336}_{-0.0337}$	1.86	4.12 ± 0.953